LIMNOLOGY and OCEANOGRAPHY

ASLO

Limnol. Oceanogr. 9999, 2020, 1–20

doi: 10.1002/lno.11639

Organic matter composition and heterotrophic bacterial activity at declining summer sea ice in the central Arctic Ocean

Judith Piontek,[1,2] Luisa Galgani ,[1,3] Eva-Maria Nöthig,[4] Ilka Peeken,[4] Anja Engel [1]*

[1]Biological Oceanography, GEOMAR Helmholtz Centre for Ocean Research Kiel, Kiel, Germany
[2]Biological Oceanography, Leibniz Institute for Baltic Sea Research Warnemünde, Rostock, Germany
[3]Department of Biotechnology, Chemistry and Pharmacy, Center for Colloid and Surface Science (CSGI) at the University of Siena, Siena, Italy
[4]Alfred Wegener Institute, Helmholtz Centre for Polar and Marine Research, Bremerhaven, Germany

Abstract

The Arctic Ocean is highly susceptible to climate change as evidenced by rapid warming and the drastic loss of sea ice during summer. The consequences of these environmental changes for the microbial cycling of organic matter are largely unexplored. Here, we investigated the distribution and composition of dissolved organic matter (DOM) along with heterotrophic bacterial activity in seawater and sea ice of the Eurasian Basin at the time of the record ice minimum in 2012. Bacteria in seawater were highly responsive to fresh organic matter and remineralized on average 55% of primary production in the upper mixed layer. Correlation analysis showed that the accumulation of dissolved combined carbohydrates (DCCHO) and dissolved amino acids (DAA), two major components of fresh organic matter, was related to the drawdown of nitrate. Nitrate-depleted surface waters at stations adjacent to the Laptev Sea showed about 25% higher concentrations of DAA than stations adjacent to the Barents Sea and in the central Arctic basin. Carbohydrate concentration was the best predictor of heterotrophic bacterial activity in sea ice. In contrast, variability in sea-ice bacterial biomass was largely driven by differences in ice thickness. This decoupling of bacterial biomass and activity may mitigate the negative effects of biomass loss due to ice melting on heterotrophic bacterial functions. Overall, our results reveal that changes in DOM production and inventories induced by sea-ice loss have a high potential to enhance the bacterial remineralization of organic matter in seawater and sea ice of the Arctic Ocean.

The Arctic is highly sensitive to anthropogenic changes in climate forcing and has warmed about two times faster than the global average over recent decades (Arctic Climate Impact Assessment 2004). Sea-ice loss is a sensitive indicator of climate change that coincides with other consequences like temperature anomalies in the Atlantic inflow and a weakening of the halocline in the eastern Eurasian Basin, referred to as "Atlantification" (Quadfasel et al. 1991; Polyakov et al. 2017). There is growing evidence for increasing phytoplankton productivity in the Arctic Ocean. Based on satellite observations, it has been estimated that Arctic net primary production increased by 30% between 1998 and 2012 mainly due to reduced ice concentration and longer growing seasons (Arrigo and van Dijken 2015). For the Eurasian Basin, estimates derived from the ^{14}C-bicarbonate method (Steemann Nielsen 1952) combined with an irradiance-based model revealed a doubling of net primary production between 1982 and 2012 (Fernández-Méndez et al. 2015). Little is known about the effects of ongoing environmental changes on the heterotrophic recycling of organic matter in the Arctic Ocean. The main proportion of oceanic carbon remineralization is carried out by heterotrophic bacteria that, consequently, largely drive the respiratory flux of CO_2 from the ocean back to the atmosphere. The low temperatures in Arctic seawater slow down enzymatic reactions and can affect the integrity and functionality of bacterial cell membranes (Feller and Gerday 2003). Yet, low seawater temperature per se does not prevent heterotrophic bacterial activity and many studies demonstrated an active microbial loop in the polar oceans (e.g., Yager and Deming 1999). Recent studies identified the availability of reactive organic matter as a major factor regulating bacterial

*Correspondence: aengel@geomar.de

Additional Supporting Information may be found in the online version of this article.

Special Issue: Biogeochemistry and Ecology across Arctic Aquatic Ecosystems in the Face of Change
Edited by: Peter J. Hernes, Suzanne Tank and Ronnie N. Glud

activity in cold oceans (Kirchman et al. 2009; Ducklow et al. 2012; Piontek et al. 2015). In particular, the availability of fresh, reactive dissolved organic matter (DOM) derived from phytoplankton exudates, sloppy feeding and viral lysis of phytoplankton cells drives the coupling between heterotrophic bacterioplankton and phytoplankton (Carlson and Hansell 2014). Source-specific optical and chemical properties of DOM revealed that the surface Arctic Ocean contains a complex DOM mixture that originates from inflowing Atlantic and Pacific waters, river runoff, and intense primary production in the summer season (Kattner et al. 1999; Gonçalves-Araujo et al. 2018). Additionally, melting sea ice provides a strong seasonal pulse of DOM into seawater that is used efficiently by bacterial communities in the surface Arctic Ocean (Niemi et al. 2014; Holding et al. 2017; Underwood et al. 2019). In general, turnover times of organic compounds in seawater are largely dependent on their molecular weight and structural complexity. Labile DOM in the surface ocean is remineralized within hours to days and pools do not exceed nanomolar concentrations. About 15–20% of the net community production in marine systems consist of semi-labile compounds with turnover times of weeks to months that accumulate in the upper mixed layer during the productive season (Carlson and Hansell 2014). Important components of labile and semi-labile organic matter are carbohydrates, amino acids, and their polymers that are produced during phytoplankton blooms and preferentially utilized by heterotrophic bacteria (Engel et al. 2011; Catalá et al. 2016; Sperling et al. 2017). Besides the chemical properties of the substrate molecules, the efficiency of bacterial organic matter remineralization may be codetermined by genetic capabilities for the synthesis of enzymes involved in hydrolysis and metabolization. Although enzymatic hydrolysis and subsequent uptake of organic compounds are considered as redundant functions in bacterial communities, Arctic bacterioplankton showed a small spectrum of polysaccharide-cleaving enzymes that may hamper the access to semi-labile DOM (Arnosti et al. 2011).

This study explores the spatial distribution of DOM along with heterotrophic bacterial activity in the marginal ice zone and the fully ice-covered part of the Eurasian Basin. The sampling took place during summer 2012, when the Arctic sea ice coverage shrank to the minimum of 3.4×10^6 km^2 (Parkinson and Comiso 2013). Concentrations of particulate and dissolved organic carbon and nitrogen, as well as concentrations and composition of carbohydrates and amino acids, were analyzed. Furthermore, rates of heterotrophic bacterial activity were determined to better characterize the cycling of fresh material in seawater and sea ice. The coupling of heterotrophic bacterial activity to the production and accumulation of organic matter in seawater and sea ice is investigated and potential effects of sea-ice loss on bacterial organic matter recycling in a warmer and fresher future Arctic Ocean are discussed.

Material and methods

Seawater sampling

Samples were collected at 28 stations during the cruise PS 80 with *RV* Polarstern from 02 August 2012 to 08 October 2012 (Fig. 1). On 16 September 2012, the Arctic sea ice reached a record minimum extent of 3.4 million km^2 (Parkinson and Comiso 2013). Stations were located between 77.4°N to 88.8°N and 17.8°E to 133.3°E in the Amundsen and Nansen Basin. Nineteen stations were located in the marginal ice zone of the Eurasian Basin, 7 of which adjacent to the Barents Sea, 2 adjacent to the Kara Sea, and 10 adjacent to the Laptev Sea (Fig. 1A). Four stations with 90–100% ice concentration were sampled in the central Arctic Basin north of 86°N. Furthermore, five stations were sampled at the shelf break. Two were located at the Barents Sea shelf break and three at the shelf break of the Laptev Sea (Fig. 1A). At each station, seawater was sampled at 3–6 depths in the upper 150 m of the water column using a rosette sampler equipped with 24 Niskin bottles. Additionally, 21 samples were collected at 500–3000 m depth. Deep-sea water was sampled at Sta. 383 and 396 in the Barents Sea sector, at Sta. 244 in the Kara Sea sector, at Sta. 263 and 341 in the Laptev Sea sector, and at Sta. 377 and 380 in the central Arctic Basin (Fig. 1A). The CTD-system was used to determine continuous depth profiles of temperature and salinity. Furthermore, a sensor for chlorophyll *a* (Chl *a*) fluorescence was mounted. Data on seawater temperature, salinity, fluorescence, inorganic nutrient concentrations, and primary production used in this study can be retrieved from the PANGAEA database (Rabe et al. 2012; Bakker 2014; Fernández-Méndez et al. 2014).

Sea-ice sampling

Sea-ice samples were obtained at eight stations referred to as Ice1 to Ice8 (Fig. 1A). Sea-ice cores were collected with a Mark II Coring System (9 cm inner diameter, Kovacs Enterprises, Roseburg, Oregon, U.S.A.). First-year ice and multiyear ice were distinguished by length and physical properties of the ice cores (Nicolaus et al. 2012; Fernández-Méndez et al. 2015). First-year ice was sampled at ice stations 1–6, while ice stations 7 and 8 were covered with multiyear ice. Ice cores were cut into sections of 10–20 cm length. Each section was vertically split with a band saw into subsamples of equal volume. For the analysis of bacterial thymidine and leucine uptake, subsamples of each section were melted in 180 mL autoclaved artificial seawater of salinity 35 to prevent the effects of osmotic shock. Depending on the length and the density of the sea-ice section, the ratio of melted sea-ice sample to artificial seawater (volume : volume) ranged from 1 : 0.6 to 1 : 2.6. A second subsample of each ice section was melted without the addition of artificial seawater for measurements of bulk salinity, the analyses of carbohydrates and amino acids and bacterial cell enumeration (Rintala et al. 2014). Bulk salinity was measured using a conductivity meter (WTW

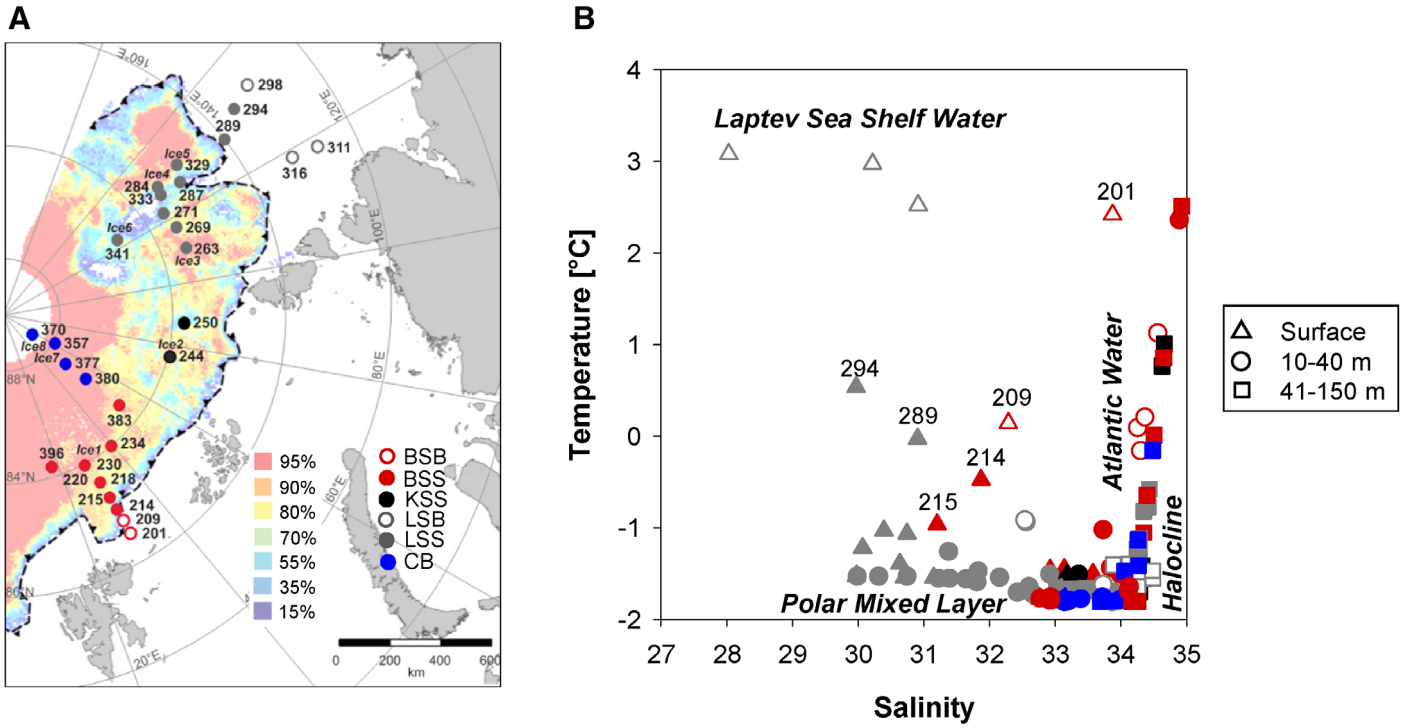

Fig 1. Sea-ice conditions and hydrography in the study area. (**A**) Ice map with stations of seawater and sea-ice sampling (BSB, Barents Sea shelf break; BSS, Barents Sea sector; KSS, Kara Sea sector; LSB, Laptev Sea shelf break; LSS, Laptev Sea sector; CB, Central Arctic Basin). (**B**) Temperature-salinity diagram of seawater sampled in different regions and depth intervals. Color code according to panel (**A**).

3300i, Xylem Analytics Germany Sales GmbH & Co. KG, WTW, Weilheim, Germany).

Melt pond sampling

At five out of the eight ice stations melt ponds could be sampled. Surface-water samples were manually collected from three to eight melt ponds per station for the analysis of amino acids, bacterial cell numbers, thymidine, and leucine uptake.

Analysis of Chl *a*

To determine the Chl *a* concentration, 1–2 L of seawater were filtered onto Whatman GF/F-filters. Filters were transferred into liquid nitrogen and kept at −80°C for later analysis by high-performance liquid chromatography (HPLC). The filters were homogenized for 20 s with 50 μL internal standard (canthaxanthin), 1.5 mL acetone and small glass beads in a Precellys® tissue homogenizer. The internal standard is used to correct for solvent and sample loss. Homogenized filters were centrifuged and the supernatant was filtered through a 0.2 μm PTFE filter (Rotilabo). An aliquot of 100 μL was transferred to the auto sampler and mixed with 1 mol L^{-1} ammonium acetate solution (ratio 1 : 1) just prior to injection into the HPLC system. Pigments including Chl *a* were then measured by reverse-phase HPLC using a Waters 600 controller equipped with a VARIAN Microsorb-MV3 C8 column (4.6 × 100 mm). Solvent A consisted of 70% methanol and 30% 1 mol L^{-1} ammonium acetate, and solvent B of 100% methanol. The gradient was modified after Barlow et al. (1997). Eluted pigments were detected by absorbance (440 nm) and fluorescence (excitation: 410 nm, emission: > 600 nm). Chl *a* was identified by comparing its retention times with those of Chl *a* standards (Sigma) and the online diode array absorbance spectra between 390 and 750 nm stored in the library. Chl *a* concentrations were quantified based on peak areas of external standards, which were spectrophotometrically calibrated using extinction coefficients published by Bidigare (1991) and Jeffrey et al. (1997).

Analysis of organic carbon and nitrogen

Particulate organic carbon (POC) and nitrogen (PN) in seawater were determined by filtering 0.5–1.0 L of seawater at low vacuum (~ 200 mbar) onto precombusted (4 h at 500°C) Whatman GF/F filters. After filtration, filters were stored at −20°C until analysis. Before analysis, filters were soaked in 0.1 mol L^{-1} HCl for removal of inorganic carbon and dried at 60°C. POC and PN concentrations were determined with a Carlo Erba CHN elemental analyzer.

For the analysis of dissolved organic carbon (DOC) and total dissolved nitrogen (TDN), 20 mL of seawater were filtered through precombusted glass fiber filters (GF/F, Whatman) into precombusted glass ampoules. Samples were acidified by addition of 20 μL 30% hydrochloric acid. Ampoules were sealed by

flame and stored at 0–4°C. Samples were analyzed by the high-temperature catalytic oxidation method (TOC-VCSH, Shimadzu) (Sugimura and Suzuki 1988; Qian and Mopper 1996). The instrument was equipped with a TNM-1 detector (Shimadzu) for the simultaneous analysis of TDN. To estimate concentrations of dissolved organic nitrogen (DON), concentrations of inorganic nitrogen were subtracted from TDN. The concentration of total organic carbon (TOC) was determined by summation of POC and DOC concentrations.

Analysis of carbohydrates and amino acids

Concentration and composition of combined carbohydrates and amino acids were determined in seawater and melted sea-ice samples. Additionally, amino acids were analyzed in melt pond samples. Samples for both components were collected in precombusted glass vials (450°C for 8 h) and stored frozen at −20°C. Seawater and melt-pond samples were filtered through a 0.45 μm syringe filter (Acrodisk, Pall Corporation), while melted sea-ice samples were collected without prefiltration.

Analysis of combined carbohydrates was conducted by high-performance anion exchange chromatography coupled with pulsed amperometric detection (ICS 3000, Dionex) using a CarboPac PA10 analytical column (Dionex). For preparation, samples were desalinated using a dialysis membrane with a 1 kDa molecular-weight cutoff (Spectra Por, Spectrum). This desalination procedure excludes carbohydrates < 1 kDa from analysis. After desalination, samples were hydrolysed with 1 mol L^{-1} hydrochloric acid and subsequently neutralized by acid evaporation under dinitrogen atmosphere and the addition of ultrapure labwater. A detailed description is given in Engel and Händel (2011). Concentrations of the neutral sugars fucose, rhamnose, arabinose, galactose, glucose, and mannose/xylose were determined. Mannose and xylose coeluted and were, therefore, quantified as a mixture. In addition to neutral sugars, concentrations of the amino sugars glucosamine and galactosamine as well as of the acidic sugars glucuronic acid and galacturonic acid were analyzed. The sum concentration of all individual neutral sugars, amino sugars, and acidic sugars is given in monomer equivalents per liter.

As seawater samples were prefiltered, the sum concentrations represent the pool of dissolved combined carbohydrates (DCCHO). The carbon-normalized yield of DCCHO (%DOC) in seawater was calculated by

$$\mathrm{DCCHO\,(\%DOC)} = \mathrm{DCCHO - C/DOC \times 100}$$

where DCCHO-C is the summed carbon concentration in all measured carbohydrates. It was calculated by multiplying the monomer concentration of each sugar with the respective number of carbon atoms and subsequent summation.

As sea-ice samples were not prefiltered, the sum concentration of individual sugars corresponds to total combined carbohydrates in sea ice, referred to as TCCHO.

Analysis of amino acids was carried out by HPLC after hydrolysis with 6 mol L^{-1} hydrochloric acid at 100°C for 20 h, neutralization and derivatization with ortho-phthaldialdehyde (Lindroth and Mopper 1979). The HPLC system (Agilent 1260) was equipped with a C18 column (Phenomenex Kinetex). Concentrations of aspartate, glutamate, serine, glycine, threonine, arginine, alanine, γ-aminobutyric acid, tyrosine, valinine, isoleucine, phenylalanine, and leucine were detected. The sum concentration of all individual amino acids is given in monomer equivalents per liter. As seawater and melt-pond samples were prefiltered, the sum concentrations represent the pool of dissolved amino acids (DAA). The carbon-normalized yield of DAA (%DOC) in seawater was calculated by

$$\mathrm{DAA\,(\%DOC)} = \mathrm{DAA - C/DOC \times 100}$$

where DAA-C is the summed carbon concentration in all measured amino acids. It was calculated by multiplying the monomer concentration of each amino acid with the respective number of carbon atoms and subsequent summation.

As sea-ice samples were not prefiltered, the sum concentration of individual amino acids corresponds to total amino acids (TAA).

Bacterial cell numbers

Samples of seawater, melt ponds, and melted sea ice were fixed on board with glutaraldehyde at 2% final concentration and stored at −20°C until analysis by flow cytometry (FACSCalibur, Becton Dickinson) within 3 months after the cruise. Bacterial cells were counted after staining with the DNA-binding dye SybrGreen I (Invitrogen). Two populations with high nucleic acid and low nucleic acid content, respectively, could be distinguished by differences in fluorescence intensity. Cell numbers were estimated after visual inspection and manual gating of the populations in the cytogram using the software CellQuest Pro (Becton Dickinson). Fluorescent latex beads (Polyscience, Becton Dickinson) were used to normalize the counted events to volume.

Cell numbers of sea-ice bacteria were converted into bacterial biomass using a mean carbon content of 0.03 pg C $bacterium^{-1}$ as determined by Gradinger and Zhang (1997) for Arctic pack ice.

Bacterial thymidine and leucine uptake

Rates of thymidine and leucine uptake were determined in seawater, melt ponds, and melted sea-ice samples to investigate heterotrophic bacterial activity. Thymidine is incorporated into newly synthesized DNA and its uptake rate is a measure for cell multiplication. Leucine is used for the build-up of new cellular proteins and the uptake rate can be used to estimate bacterial biomass production. Uptake rates were determined using tritium-labeled tracers. ^{3}H-thymidine and ^{3}H-leucine with specific activities of 70 Ci $mmol^{-1}$ and 100 Ci $mmol^{-1}$, respectively, were added to separate incubations.

For seawater and melt ponds, 1.5 mL of sample were incubated with ^{3}H-thymidine and ^{3}H-leucine at 10 nmol L^{-1} and 20 nmol L^{-1} final concentration, respectively. Triplicate samples were incubated along with a poisoned control for 3–8 h close to in situ temperature. Incubation times were adjusted for the individual stations based on the sensor-derived Chl *a* fluorescence that was determined during the CTD cast. Samples were processed by the centrifuge method according to Smith and Azam (1992). Briefly, samples were centrifuged at $14{,}000 \times g$ after the addition of cold 5% trichloroacetic acid to obtain a cell pellet that was afterward washed twice with cold 5% trichloroacetic acid. Incorporation into the trichloroacetic acid-insoluble fraction was measured by liquid scintillation counting after resuspension of the cell pellet in scintillation cocktail (Ultima Gold AB, Perkin Elmer). The bacterial biomass production in seawater samples was estimated from leucine uptake applying the conversion factor of 1.5 kg C mol leucine^{-1}, assuming no intracellular isotope dilution (Simon and Azam 1989). The bacterial carbon demand in seawater was estimated assuming a bacterial growth efficiency of 20% (del Giorgio and Cole 1998). Thymidine uptake was converted into cell production using the factor 1.3×10^{18} cells mol thymidine^{-1} (Riemann et al. 1990).

The Q_{10} factor for leucine and thymidine uptake was determined from a subset of 29 seawater samples. For each sample, two series of three replicate samples were spiked with the radioactive tracers as described above and placed at 0°C and 4°C, respectively, for equal incubation times. The Q_{10} factor was then estimated by

$$Q_{10} = (R_4/R_0)^{2.5}$$

where R_4 and R_0 are the rates determined at 4°C and 0°C, respectively. The ratio R_4/R_0 was derived from the slopes of regression lines of rates at 0°C against rates at 4°C.

Sea-ice samples melted in artificial seawater (see above) were spiked with ^{3}H-thymidine and ^{3}H-leucine at final concentrations of 20 nmol L^{-1} and 40 nmol L^{-1}, respectively. Melted samples of two to five ice-core segments with similar thickness were pooled with equal proportions, resulting in incubations for the top, middle, and bottom part of the ice core. Duplicates were incubated for 13–21 h at 0°C along with a poisoned control. After incubation, samples were filtered onto 0.2 μm polycarbonate filters (Millipore) that were rinsed two times with 5 mL cold 5% TCA. Filters were placed in a scintillation vial and radio-assayed after the addition of scintillation cocktail (Ultima Gold AB, Perkin Elmer). To derive rates per sea-ice volume, the rates determined for sea-ice samples melted in artificial seawater were multiplied with the factor d to correct for the dilution according to

$$d = v_m/(v_m - v_{ASW})$$

where v_m is the total volume after sea-ice melting (mL) and v_{ASW} is the volume of added artificial seawater (ASW) (mL). Bacterial biomass production in sea ice was estimated from thymidine uptake using conversion factors of 2.09×10^{18} cells mol thymidine^{-1} and 0.03 pg C bacterium^{-1} (Smith and Clement 1990; Gradinger and Zhang 1997).

Statistical analysis

Differences in organic matter concentrations, bacterial abundance, and activity between the investigated areas of the Eurasian Basin were tested for significance by ANOVA on ranks combined with post hoc Mann–Whitney rank sum test. Differences between samples collected at ≤ 40 m and at 41–150 m were tested by the Wilcoxon rank sum test for the individual sampling areas Barents Sea sector, Laptev Sea sector, and central Arctic Basin. Significance was accepted for $p < 0.05$.

Principal component analysis (PCA) was conducted with the R packages FactoMineR for analysis and Factoextra for visualization (Lê et al. 2008).

Results

Hydrographic characteristics of sampling regions

Seawater samples can be assigned to different water masses of the Arctic Ocean based on temperature and salinity characteristics according to Rudels (2009) (Fig. 1B). Highest salinities up to 34.9 were measured at 10–40 m depth at the Barents Sea shelf break and in the adjacent Barents Sea sector, indicating Atlantic Water inflow from the Norwegian Sea into the Arctic Ocean. Surface salinity (≤ 10 m) was reduced to 31.9–33.8 at stations located close to the ice margin (Sta. 201, 209, 214, and 215) (Fig. 1A,B). Profiles of Sta. 214 and 215 in the Barents Sea sector showed enhanced water column stratification and a thin upper mixed layer of about 15 m depth (Supporting Information Fig. S1). Samples collected at 0–40 m in the Laptev Sea sector and in the central Arctic Basin reveal temperature and salinity characteristics of the Polar Mixed Layer that develops during progressive heat exchange with the atmosphere and freshening by river runoff. The water column of stations located at the Laptev Sea shelf break and beyond in the Laptev Sea sector was strongly stratified with a mixed layer depth of about 20–30 m (Supporting Information Fig. S1). Surface samples of three stations located at the Laptev Sea (Sta. 298, 311, 316) showed typical features of Laptev Sea Shelf Water with salinities of 28.0–30.9 in coincidence with high temperatures of 2.5–3.1°C (Fig. 1A,B). Most samples collected at 41–150 m represent upper and lower halocline water with negative temperatures at salinities of 33.3–34.5 in all investigated regions (Fig. 1B).

Organic matter in seawater

Comparing the sampling regions in the Eurasian Basin revealed no spatial differences in POC and PN concentrations. POC : PN ratios ranged from 5.1 to 9.7 and were similar in all

investigated regions. POC concentrations were significantly higher in the upper water column than at 41–150 m depth in the Laptev Sea Sector (Mann–Whitney ranked sum test, $p = 0.0001$) but not in the other regions. PN concentrations in the upper (≤ 40 m) and lower (41–150 m) water column were similar in all regions of the Eurasian Basin. The contribution of POC to TOC showed a broad range from 3.3% to 22.8% without significant differences between Barents Sea sector, Laptev Sea sector, and central Arctic Basin (Table 1).

Concentrations of DOM revealed spatial variability within and between the sampling regions (Table 1). Within the sampling regions, highest variability was determined in the upper water column (≤ 40 m) of the Barents Sea sector. Concentrations of DCCHO and DAA significantly decreased with depth in the Laptev Sea Sector and the central Arctic Basin, while the upper and lower water column in the Barents Sea sector showed similar concentrations (Table 1). A comparison of the different sampling areas in the Arctic Basin revealed significantly higher DOC and DAA concentrations in the upper water column of the Laptev Sea sector compared to the Barents Sea sector (Table 1) (ANOVA on ranks, $p < 0.05$; post hoc Mann–Whitney rank sum test, $p \leq 0.001$). Concentrations of both constituents were inversely related to salinity in the upper 40 m of the Laptev Sea sector (Fig. 2). Three stations located close to the ice margin in the Laptev Sea sector (Sta. 284, 287, and 289) showed larger deviations of DOC concentrations from the regression line that were likely induced by freshening of surface waters by intense sea-ice melting. Theoretical dilution lines for DOC and DAA were derived from concentrations published for the Lena River by Lara et al. (1998) combined with concentrations determined at maximum salinity in the Laptev Sea sector in this study. The dilution line of DOC deviates only slightly from the regression line. In contrast, the extrapolated DAA concentration of 830 nmol L^{-1} for the freshwater endmember is far below DAA concentrations in the Lena delta (average DAA concentration 3.5 μmol L^{-1}; Lara et al. 1998) (Fig. 2).

Across all sampling regions and depths, concentrations of DCCHO and DAA were inversely related to nitrate concentrations (Fig. 3A). The correlation coefficients further increased when samples collected in the Barents Sea sector and across the Barents Sea shelf break were not included. No such relationship was determined for silicate and DCCHO and DAA concentrations, respectively (Fig. 3B).

On average, 2.8% and 0.8% of DOC in the upper 150 m of the water column were contained in DCCHO and DAA, respectively. These fractions were reduced to 2.2% and 0.4% for DCCHO and DAA, respectively, in deep ocean samples collected at 500–3000 m (Table 1). The molecular composition shows that DCCHO were dominated by glucose (22–80 mol%) and mannose/xylose (14–55 mol%). From surface to the deep ocean, seawater became depleted in rhamnose, arabinose, and galacturonic acid and proportions of fucose and galactose were strongly reduced (Table 2). The DAA composition in seawater was characterized by the dominance of glycine (28–46 mol%)

Table 1. Organic matter and Chl *a* concentrations in the sampling regions of the Eurasian Basin.

Region/ depth	DOC (μmol L^{-1})	DON (μmol L^{-1})	DOC : DON	DCCHO (nmol L^{-1})	DCCHO (%DOC)	DAA (nmol L^{-1})	DAA (%DOC)	POC (μmol L^{-1})	POC (%TOC)	PN (μmol L^{-1})	POC : PN	Chl *a* (mg m^{-2})
≤40 m	*a, b*	*b*				*b, c*						*c*
Barents Sea Sector	63 (56–153)	6.3 (3.6–11.6)	11.7 (5.7–28.6)	354 (238–1179)	2.7 (1.3–10.7)	165 (141–369)	0.8 (0.4–2.3)	8.0 (6.0–19.4)	10.7 (5.0–22.8)	1.3 (0.9–3.3)	7.3 (6.3–8.6)	10.7 (8.4–43.3)
Laptev Sea Sector	107 (63–122)	7.9 (7.0–10.6)	13.0 (10.2–17.0)	428 (269–666)	2.3 (1.5–4.4)	219 (167–285)	0.7 (0.6–1.4)	10.2 (5.7–24.0)	10.5 (5.4–17.1)	1.8 (0.8–3.7)	7.4 (5.1–9.7)	14.2 (9.6–16.0)
Central Basin	85 (66–163)	7.4 (4.8–8.8)	11.9 (8.0–25.6)	389 (237–746)	2.9 (1.5–5.0)	172 (152–244)	0.6 (0.4–1.0)	7.9 (3.2–16.4)	8.9 (3.3–16.4)	1.3 (0.5–2.8)	7.3 (6.0–8.8)	8.4 (6.9–10.0)
41–150 m	*b*											
Barents Sea Sector	60 (57–74)	5.7 (2.7–18.2)	11.8 (3.2–25.3)	316 (206–888)	2.9 (1.7–7.9)	177 (115–344)	0.9 (0.6–2.0)	7.0 (3.3–10.1)	9.1 (5.3–14.8)	1.1 (0.5–1.6)	7.5 (6.9–9.3)	
Laptev Sea Sector	73 (56–99)	6.9 (4.7–9.2)	12.1 (7.2–15.9)	273 (182–526)	2.3 (1.4–3.9)	137 (92–188)	0.6 (0.4–0.8)	6.7 (3.7–10.9)	7.6 (5.1–14.5)	1.1 (0.4–2.0)	7.3 (5.8–10.1)	
Central Basin	70 (59–93)	7.0 (4.3–9.3)	11.6 (7.0–14.7)	271 (185–325)	2.4 (1.6–2.7)	138 (114–156)	0.6 (0.5–0.7)	6.2 (4.4–27.5)	8.3 (5.1–22.8)	1.0 (0.7–1.6)	7.2 (6.6–22.7)	
500–3000 m	*57 (46–96)*	*7.7 (5.3–10.6)*	*8.1 (5.9–18.1)*	*226 (141–566)*	*2.2 (1.6–6.1)*	*83 (63–157)*	*0.4 (0.3–0.6)*	*Na*	*Na*	*Na*	*Na*	

The median is given as well as minimum and maximum values in parentheses (DOC, dissolved organic carbon; DON, dissolved organic nitrogen; DCCHO, dissolved combined carbohydrates; POC, particulate organic carbon; PN, particulate nitrogen; *Na*: not available). Labels denote significant differences between the Barents Sea Sector, the Laptev Sea Sector, and the central Arctic Basin as derived from ANOVA on ranks and post hoc Wilcoxon rank sum test (*a*: $p < 0.05$ for Barents Sea Sector vs. central Arctic Basin, *b*: $p < 0.05$ for Barents Sea sector vs. Laptev Sea sector, *c*: $p < 0.05$ for Laptev Sea sector vs. central Arctic Basin).

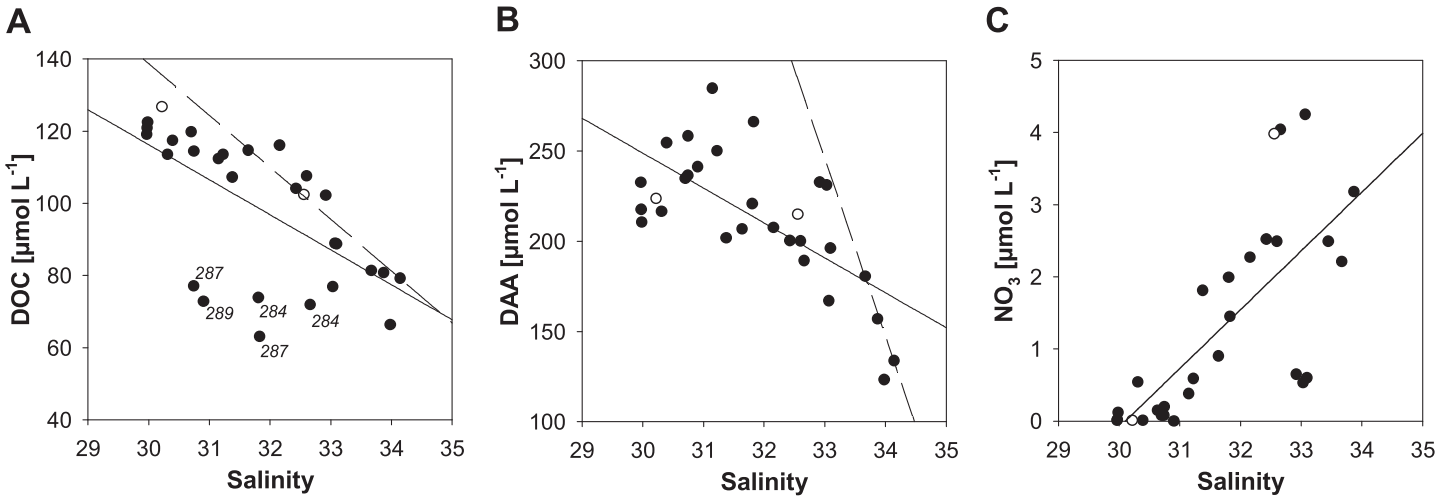

Fig 2. Concentrations of dissolved organic carbon (DOC) (**A**), dissolved amino acids (DAA) (**B**), and nitrate (NO_3) (**C**) at ≤ 40 m related to salinity at the Laptev Sea shelf break (open symbols) and in the Laptev Sea sector (closed symbols). Concentrations of DOC and DAA for the freshwater endmember were derived from Lara et al. (1998) to construct the dilution lines (dashed). Regression lines (solid): (**A**) $y = -9.7x + 407$, $r^2 = 0.41$, $p = 0.0002$, $n = 29$, (**B**) $y = -19.4x + 830$, $r^2 = 0.47$, $p < 0.0001$, $n = 29$, (**C**) $y = 0.81x - 24.5$, $r^2 = 0.53$, $p < 0.0001$, $n = 29$. Numbers given in panel (A) denote stations of seawater sampling.

that showed increasing proportions with depth. Aspartate, serine, threonine, alanine, and glutamate contributed 9–16 mol % each to DAA (Table 3). PCA was conducted to test for spatial differences in DCCHO and DAA composition in the upper water column (≤ 40 m) (Fig. 4). Most samples clustered together, revealing no region-specific DCCHO and DAA composition. However, PCA of DCCHO composition separated a subset of samples originating from the Barents Sea sector and the Barents Sea shelf break on PC2 (Fig. 4A). Stations 201, 209, 214, and 218, which were located in the transition zone from open waters at the Barents Sea shelf break to the ice margin in the Eurasian Basin, showed higher proportions of rhamnose (8.1 mol%) and arabinose (4.1 mol%), when compared with the median of all samples collected at 0–40 m depth (rhamnose: 4.1 mol%, arabinose: 0.9%). PCA revealed also compositional differences in DAA between four samples collected at the Barents Sea shelf break and in the adjacent Barents Sea sector (Sta. 201, 214, 230, and 234) and all other samples. Three out of these four samples were characterized by elevated proportions of glutamate (15 mol%) and serine (17 mol%) compared to the median of all surface samples (glutamate: 9 mol%, serine: 10 mol%) (Fig. 4B).

Heterotrophic bacterial activity in seawater and its coupling to phytoplankton production

Uptake rates of leucine ranged from 0.98 to 18.24 pmol L^{-1} h^{-1} and conversion into bacterial biomass production resulted in 0.01–1.17 μg C L^{-1} d^{-1} (Table 4). Bacterial cell production estimated from thymidine uptake ranged from 1.3×10^3 to 1.6×10^5 cells mL^{-1} d^{-1} (Table 4). Bacterial activity showed significant differences between the sampling regions in the Eurasian Basin. The bacterial uptake of leucine in the upper water column (≤ 40 m) was significantly higher at stations in the Barents Sea sector and in the Laptev Sea sector than in the central Arctic Basin, revealing higher bacterial biomass production in the marginal ice zone than in the fully ice-covered part of the Eurasian Basin. Communities in the Barents Sea sector and in the Laptev Sea sector showed similar uptake rates and bacterial cell numbers in surface waters (≤ 40 m), while rates and abundances at 41–150 m were significantly higher in the Barents Sea sector (Table 4). Ratios of leucine to thymidine uptake in the upper water column were significantly higher in the Barents Sea sector than in the Laptev Sea sector and the central Arctic Basin. This indicates higher bacterial protein production relative to DNA synthesis in the Laptev Sea sector and the central Arctic Basin compared to the Barents Sea sector (ANOVA on ranks, $p < 0.05$; post hoc Mann–Whitney rank sum test, $p \leq 0.05$) (Table 4).

Stations in the Laptev Sea sector showed significantly higher Chl *a* concentrations than those in the Barents Sea sector and the central Arctic Basin, indicating higher standing stocks of phytoplankton at the time of our study (ANOVA on ranks, $p < 0.05$; post hoc Mann–Whitney rank sum test, $p \leq 0.05$) (Table 1). In order to investigate the coupling between heterotrophic bacteria and phytoplankton, bacterial biomass production was depth-integrated over 50 m to encompass the upper mixed layer and the euphotic zone at all stations. Correlation analysis of log-log transformed data revealed that bacterial production was significantly related to both Chl *a* concentrations and primary production (Fig. 5A,B). Ratios of bacterial production to primary production ranged from 0.03 to 0.23 with a mean ratio of 0.11 (Fig. 5C).

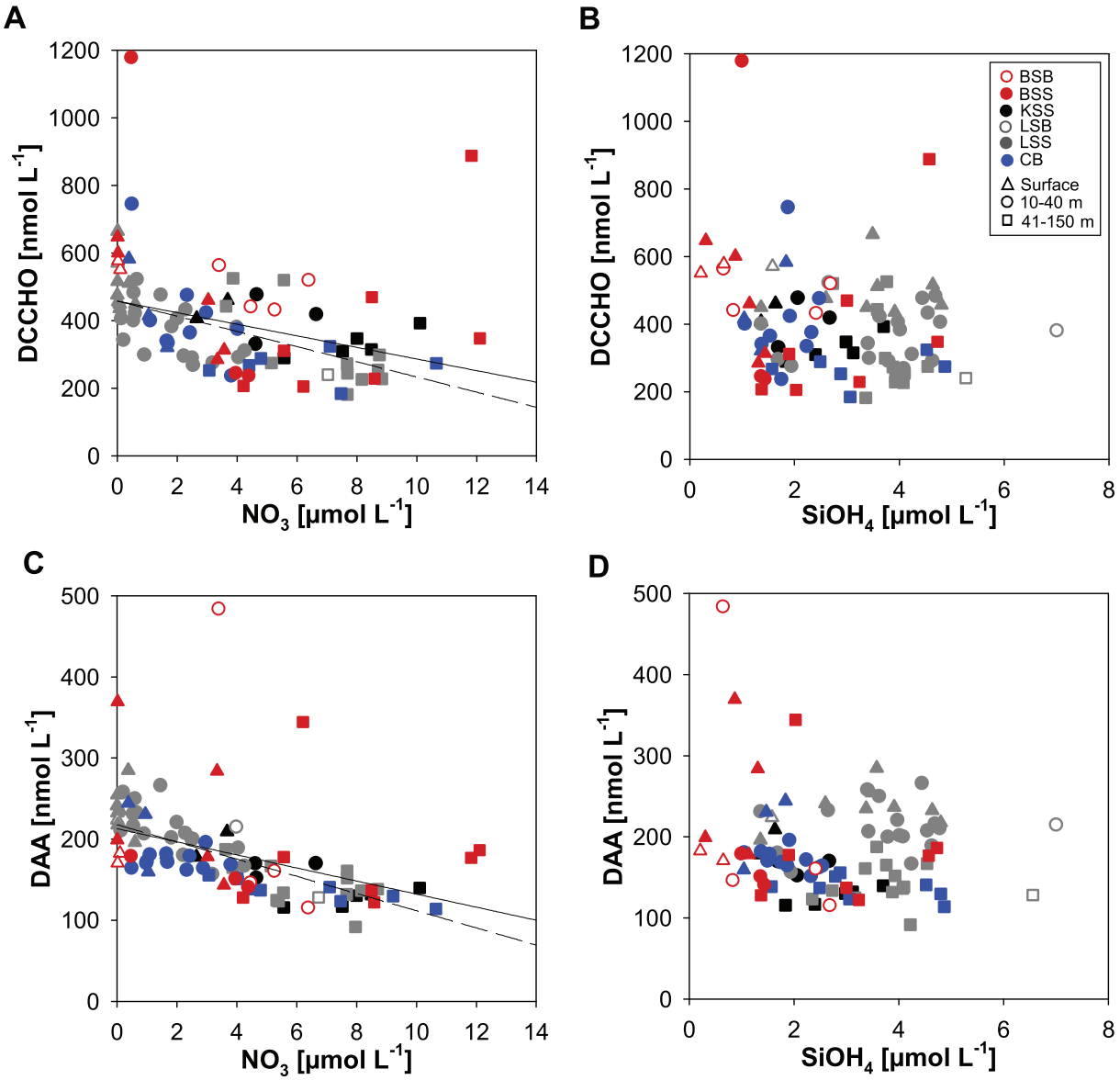

Fig 3. Concentrations of dissolved combined carbohydrates (DCCHO) (**A**, **B**) and DAA (**C**, **D**) related to nitrate (NO_3) and silicate ($SiOH_4$) concentrations in seawater. Lines are shown for significant regressions. Regression analyses were conducted with the whole data set (solid lines) and without samples collected at the Barents Sea shelf break and in the adjacent Barents Sea sector (dashed lines) (BSB, Barents Sea shelf break; BSS, Barents Sea sector; KSS, Kara Sea sector; LSB, Laptev Sea shelf break; LSS, Laptev Sea sector; CB, Central Arctic Basin). (**A**) All samples: $y = -17.2x + 459$, $r^2 = 0.13$, $p < 0.0002$, $n = 100$; without Barents Sea sector and shelf break: $y = -22.5x + 459$, $r^2 = 0.36$, $p < 0.0001$, $n = 67$; (**C**) All samples: $y = -8.1x + 213$, $r^2 = 0.21$, $p < 0.0001$, $n = 108$; without Barents Sea shelf break and sector: $y = -10.6x + 218$, $r^2 = 0.58$, $p < 0.0001$, $n = 75$.

Assuming a bacterial growth efficiency of 20%, the mean ratio suggests that on average 55% of primary production was remineralized by heterotrophic bacterioplankton on short time scales. Highest ratios of 0.19–0.23 imply that primary production was completely consumed by heterotrophic bacterioplankton at Sta. 201, 234, 333, and 383 and presumably no fresh organic matter accumulated in the upper mixed layer at the time of our study. Changes in ratios of bacterial production to primary production were largely driven by changes in primary production. Ratios of bacterial production to primary production showed the tendency to decrease with increasing primary production, suggesting a lower percentage of bacterial remineralization at stations with intense phytoplankton growth (Fig. 5C).

An experimental temperature increase from 0°C to 4°C in short-term incubations of 3–8 h had a consistent positive effect on bacterial leucine and thymidine uptake. Regression lines reveal an increase in leucine and thymidine uptake by a factor of 1.40 (± 0.04) and 1.29 (± 0.04) for leucine and thymidine, respectively (Fig. 5D). This factorial increase at a 4°C

Table 2. Sum concentration and monomer composition of dissolved combined carbohydrates in seawater and total combined carbohydrates in sea ice.

			mol%									
Sample type	Total (nmol L^{-1})	CHO : AA	Fu	Rha	Galac-amin	Arab	Glu-amin	Galac	Glu	Man/Xyl	Galac-URA	Glu-URA
Seawater												
0–40 m	407 (237–1179)	2.1 (1.0–6.6)	6.8 (3.7–11)	4.1 (0.9–16)	0.4 (0.0–1.0)	0.9 (0.0–7.7)	6.9 (3.5–9.8)	9.0 (2.8–15)	37 (22–71)	30 (14–45)	0.8 (0.0–3.5)	0.0 (0.0–1.0)
41–150 m	295 (182–888)	2.1 (0.6–5.0)	5.3 (1.8–9.0)	2.5 (0.0–14)	0.4 (0.0–1.0)	0.5 (0.0–12)	5.4 (1.9–8.3)	6.7 (2.1–15)	46 (24–74)	30 (17–49)	0.2 (0.0–2.3)	0.0 (0.0–0.0)
500–3000 m	226 (141–566)	2.6 (1.5–5.7)	3.4 (1.5–5.7)	0.0 (0.0–3.6)	0.0 (0.0–1.0)	0.0 (0.0–0.3)	3.8 (1.9–6.0)	3.8 (1.1–6.1)	49 (34–80)	35 (15–55)	0.0 (0.0–0.8)	0.0 (0.0–0.0)
Sea ice	1015 (285–3721)	3.0 (0.2–12.6)	1.6 (0.3–5.6)	0.3 (0.0–0.9)	0.0 (0.0–0.0)	1.9 (0.0–5.6)	1.2 (0.0–3.9)	4.0 (1.0–8.8)	68 (42–87)	18 (5.8–45)	0.6 (0.0–2.2)	2.0 (0.6–4.3)

The median is given as well as minimum and maximum values in parentheses (CHO, carbohydrates; AA, amino acids; Fu, fucose; Rha, rhamnose; Galac-amin, galactosamine; Arab, arabinose; Glu-amin, glucosamine; Galac, galactose; Glu, glucose; Man/Xyl, mannose/xylose; Galac-URA, galacturonic acid; Glu-URA, glucuronic acid).

Table 3. Sum concentration and monomer composition of dissolved amino acids in seawater and melt ponds and total amino acids in sea ice.

		mol%												
Sample type	Total (nmol L^{-1})	AsX	GlX	Ser	Gly	Thr	Arg	Ala	GABA	Tyr	Val	Iso	Phe	Leu
Seawater														
0–40 m	182 (116–484)	16 (12–19)	8.9 (7.4–15)	10 (8–19)	33 (28–39)	9.3 (4.5–12)	0.9 (0.1–1.8)	13 (10–14)	1.0 (0.4–3.6)	0.7 (0.1–1.3)	2.3 (1.6–3.0)	1.3 (0.9–2.0)	1.1 (0.6–1.7)	1.7 (0.9–2.9)
41–150 m	138 (92–344)	15 (12–18)	8.4 (6.6–15)	10 (7–18)	36 (31–41)	10 (5.9–12)	0.7 (0.0–4.6)	13 (8.7–14)	1.1 (0.2–1.5)	0.5 (0.0–1.3)	2.0 (1.3–4.2)	1.2 (0.6–2.7)	0.9 (0.5–1.9)	1.3 (0.4–4.1)
500–3000 m	83 (63–157)	13 (10–15)	7.2 (5.3–13)	8.9 (6.8–17)	40 (32–46)	10 (7.5–15)	0.6 (0.0–1.5)	13 (10–15)	1.2 (0.6–1.8)	0.3 (0.0–1.1)	1.6 (1.2–2.3)	1.0 (0.4–1.5)	1.1 (0.3–1.8)	0.8 (0.3–2.9)
Sea ice	289 (65–3319)	10 (6.6–14)	23 (19–35)	17 (5.8–24)	19 (8.7–23)	6.0 (3.7–7.2)	1.3 (0.5–13.6)	10 (8–13)	0.9 (0.2–18)	1.2 (0.0–2.1)	3.3 (1.0–5.9)	2.1 (1.4–2.9)	1.4 (0.8–2.3)	3.0 (2.2–5.1)
Melt pond	191 (86–2473)	15 (12–20)	12 (10–15)	12 (7.6–18)	4.3 (1.9–5.1)	20 (15–30)	8.0 (5.5–10.7)	12 (10–15)	1.2 (0.7–2.2)	1.5 (1.2–2.0)	4.6 (2.9–5.5)	3.1 (1.7–4.8)	1.9 (0.8–3.1)	4.1 (2.1–6.3)

The median is given as well as minimum and maximum values in parentheses (AsX, aspartate; GluX, glutamate; Ser, serine; Gly, glycine; Thr, threonine; Arg, arginine; Ala, alanine; GABA, γ-aminobutyric acid; Tyr, tyrosine; Val, valinine; Iso, isoleucine; Phe, phenylalanine; Leu, leucine).

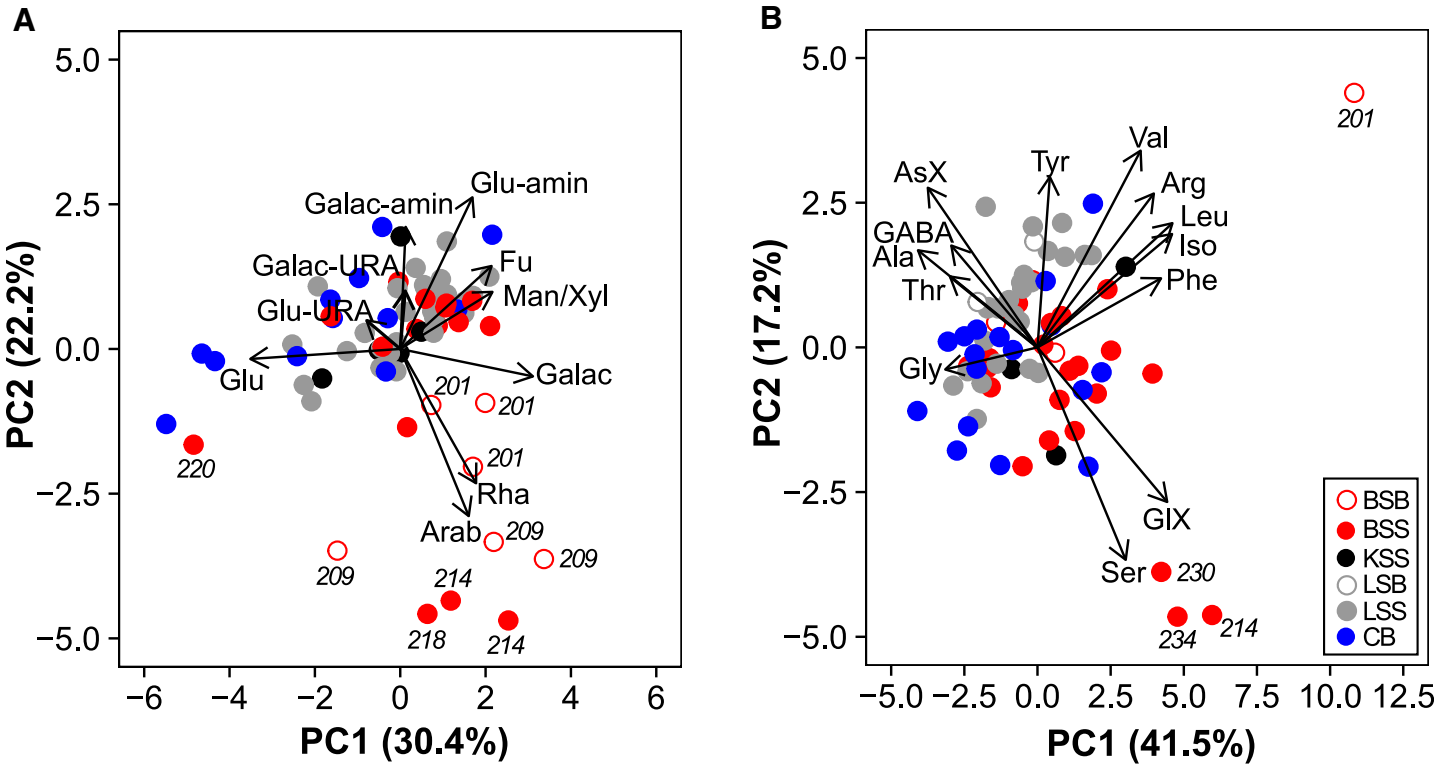

Fig 4. Principal component analysis of monomer composition of dissolved combined carbohydrates (DCCHO) (**A**, **B**) and dissolved amino acids (DAA) (**B**) in seawater ≤ 40 m. (**A**) Fu, fucose; Rha, rhamnose; Galac-amin, galactosamine; Arab, arabinose; Glu-amin, glucosamine; Galac, galactose; Glu, glucose, Man/Xyl, mannose/xylose; Galac-URA, galacturonic acid; Glu-URA, glucuronic acid. (**B**) AsX, aspartate; GluX, glutamate; Ser, serine; Gly, glycine; Thr, threonine; Arg, arginine; Ala, alanine; GABA, γ-aminobutyric acid; Tyr, tyrosine; Val, valinine; Iso, isoleucine; Phe, phenylalanine; leu, leucine. Sampling regions (**A**, **B**): BSB, Barents Sea shelf break; BSS, Barents Sea sector; KSS, Kara Sea sector; LSB, Laptev Sea shelf break; LSS, Laptev Sea sector; CB, Central Arctic Basin.

temperature difference corresponds to Q_{10}-values of 2.3 and 1.9 for leucine and thymidine uptake, respectively.

Organic matter and heterotrophic bacterial activity in sea ice and melt ponds

Ice-core profiles revealed a highly variable vertical distribution of TCCHO and TAA concentrations (Fig. 6). In most ice cores, bottom layers showed the highest concentrations of TCCHO but elevated concentrations were also detected in several surface and middle ice sections (Fig. 6). Carbohydrates in sea ice were dominated by glucose (42–87 mol%) and mannose/xylose (6–45 mol%). Sea-ice carbohydrates also included a substantial proportion of glucuronic acid (0.6–4.3 mol%). Glutamate (19–35 mol%) was the most abundant amino acid in sea-ice samples that were further enriched in serine (6–24 mol%).

Concentrations of DAA in melt ponds were in the range of seawater samples collected at ≤ 40 m. Melt pond samples showed a more even amino acid composition than seawater samples and included higher proportions of threonine (15–30 mol%) and arginine (6–11 mol%) (Table 3).

Sea-ice samples contained on average 1.0×10^5 bacteria mL^{-1} (Fig. 6; Supporting Information Table S1). The vertical distribution of bacterial cells in sea ice was directly related to bulk salinity that increased from surface to bottom ice (Fig. 6; Supporting Information Table S2). Depth-integrated bacterial biomass in ice cores ranged from 0.8 to 11.6 mg C m^{-2}. It was significantly related to the ice core length and, consequently, to ice thickness (r^2 = 0.98, $p < 0.001$, n = 8) (Table 5, Supporting Information Table S3). Thymidine and leucine uptake in sea ice did not show consistent vertical patterns. Leucine uptake was directly related to CCHO concentrations and showed higher variation within and between ice cores than thymidine uptake. Bacterial biomass production in sea ice estimated from depth-integrated thymidine uptake averaged 18.8 μg C m^{-2} h^{-1} (Table 5; Fig. 6). Assuming a bacterial growth efficiency of 24% (Nguyen and Maranger 2011), this corresponds to an average bacterial carbon demand of 78.2 μg C m^{-2} h^{-1} (Table 5). Sea-ice primary production was estimated to be 2.2 mg C m^{-2} d^{-1} at the time of our study (Fernández-Méndez et al. 2015). Hence, the bacterial carbon demand corresponded to approximately 85% of primary production in sea ice during late summer. Ranges of bacterial abundances, leucine, and thymidine uptake in melt ponds were similar to those in bottom sea ice and higher than in the top and middle sections of the ice cores (Table 6).

Table 4. Bacterial abundance and activity in the sampling regions of the Eurasian Basin.

Region/depth	Bacteria ($\times 10^5$ cells mL^{-1})	%HNA cells	Leu uptake (pmol L^{-1} h^{-1})	Leu uptake (amol cell^{-1} h^{-1})	Thy uptake (pmol L^{-1} h^{-1})	Thy uptake (amol cell^{-1} h^{-1})	Leu : Thy
≤40 m		*a*	*a, c*	*c*	*a*		*a, c*
Barents Sea Sector	6.1 (2.20–17.9)	56 (40–69)	6.48 (1.78–18.24)	0.24 (0.04–1.23)	0.95 (0.34–5.13)	0.04 (0.01–0.20)	6.7 (3.0–8.2)
Laptev Sea Sector	6.0 (2.05–9.07)	55 (41–69)	7.45 (1.00–12.44)	0.30 (0.09–0.44)	0.81 (0.10–1.63)	0.03 (0.01–0.05)	7.9 (6.2–18.7)
Central Eurasian Basin	4.2 (2.43–7.12)	48 (37–58)	3.28 (0.98–5.09)	0.15 (0.08–0.28)	0.32 (0.11–1.30)	0.02 (0.01–0.05)	8.8 (3.7–14.0)
41–150 m	*b*	*b*	*a, b*	*b*	*b, c*	*b*	
Barents Sea Sector	2.9 (1.11–8.45)	65 (50–69)	2.35 (0.46–13.69)	0.23 (0.03–0.39)	0.33 (0.06–2.98)	0.02 (0.01–0.08)	6.5 (3.5–13.7)
Laptev Sea Sector	1.5 (0.87–2.83)	63 (55–72)	0.57 (0.30–0.97)	0.09 (0.05–0.17)	0.07 (0.04–0.21)	0.01 (0.01–0.03)	8.1 (2.6–18.3)
Central Eurasian Basin	1.9 (0.89–4.17)	60 (52–67)	0.68 (0.23–1.41)	0.09 (0.03–0.12)	0.09 (0.07–0.30)	0.02 (0.01–0.05)	6.0 (1.4–10.8)

The median is given as well as minimum and maximum values in parentheses (HNA, high-nucleic acid, Leu, leucine; Thy, thymidine). Labels denote significant differences between the Barents Sea Sector, the Laptev Sea Sector, and the central Arctic Basin as derived from ANOVA on ranks and post hoc Wilcoxon rank sum test (*a*: $p < 0.05$ for Barents Sea sector vs. central Arctic Basin, *b*: $p < 0.05$ for Barents Sea sector vs. Laptev Sea sector, *c*: $p < 0.05$ for Laptev Sea sector vs. central Arctic Basin).

Both thymidine and leucine uptake showed higher variability in melt ponds than in sea ice (Table 5).

Discussion

Importance of nitrate availability for the accumulation of semi-labile DOM in the Eurasian Basin

Reactive DOM in the open ocean is mainly derived from phytoplankton primary production and released by phytoplankton exudation, bacterial particle solubilization, viral lysis of cells, and sloppy feeding by zooplankton (Carlson and Hansell 2014). It contains elevated proportions of carbohydrates and amino acids, which are important semi-labile resources for heterotrophic bacterial growth (Kirchman et al. 2001; Piontek et al. 2011). The high-molecular weight and structural complexity of polymers result in turnover times of weeks to months and, thereby, to surface accumulation during the productive season. Our results reveal an inverse relationship between nitrate and DCCHO and DAA concentrations, respectively, suggesting that the utilization of inorganic nitrogen for primary production was proportional to the release and subsequent accumulation of semi-labile DOM during the summer season. Maximum concentrations of DCCHO and DAA were determined in nitrate-depleted surface samples, implying that nitrate availability limited the build-up of DOM in high-light regimes of open waters and regions with low ice concentration. The slopes of the regression lines suggest an accumulation of about 8 nmol DAA and 17 nmol DCCHO per micromole nitrate consumption. A total nitrate consumption of 119 ± 46 mmol m^{-2} was estimated for the productive season of the year 2012 in the Eurasian Basin (Fernández-Méndez et al. 2015). Based on these values, it can be estimated that about 952 ± 368 μmol DAA m^{-2} and 2.0 ± 0.8 mmol DCCHO m^{-2} accumulated in the upper mixed layer. These estimates suggest that about 25% of DAA and DCCHO in surface waters of the Eurasian Basin was derived from primary production by Arctic phytoplankton during the recent summer season and, consequently, about 75% of the two components likely originated from inflowing Atlantic Water potentially mixed with remnants from the previous Arctic summer season.

Our results imply that potential changes in nitrate fluxes are of high relevance for DOM production and accumulation at decreasing sea-ice concentrations and prolonged growing seasons in the Arctic Ocean. Inorganic nutrients in Atlantic Water entering the Eurasian Basin show higher N : P ratios than the Pacific inflow to the Amerasian Basin (Jones et al. 1998). The higher load of inorganic nitrogen in the Eurasian Basin remains largely submerged under the fresher Arctic surface water, although the Arctic halocline may weaken in response to future climate change (Polyakov et al. 2018). During the last three decades, significant changes in the nitrate supply by Atlantic Water have been observed. The mean winter nitrate concentration in the southwestern Barents Sea decreased by 0.7 μmol L^{-1} yr^{-1} (Oziel et al. 2017). Nutrient

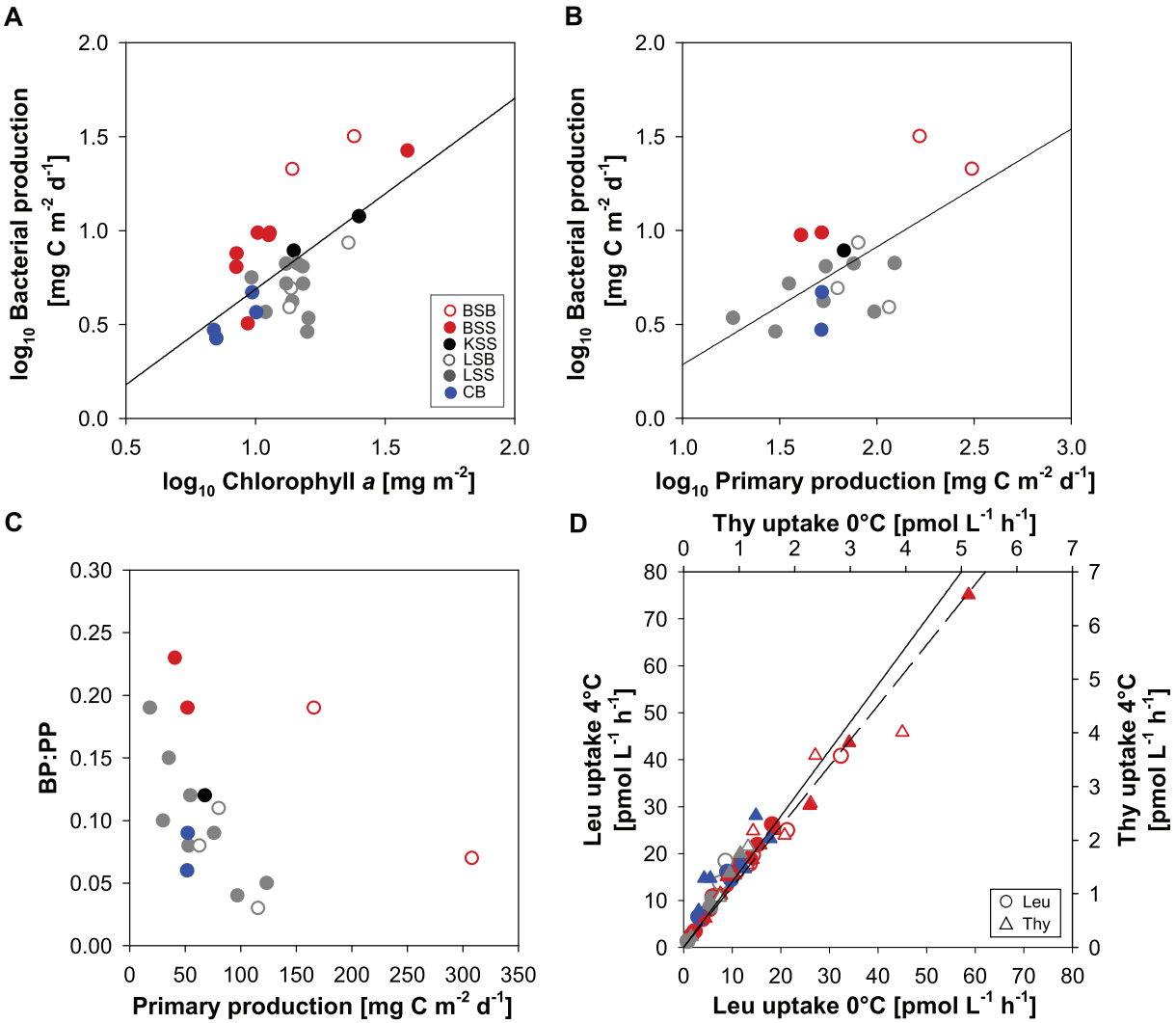

Fig 5. Control of bacterial production (BP) by phytoplankton standing stocks (**A**), primary production (PP) (**B**, **C**), and temperature (**D**). Regression lines: (**A**) $y = 1.0x - 0.33$, $r^2 = 0.38$, $p = 0.0005$, $n = 28$, (**B**) $y = 0.63x - 0.34$, $r^2 = 0.41$, $p = 0.0043$, $n = 18$, (**D**) Leucine (Leu): $y = 1.4x$, $r^2 = 0.93$, $p < 0.0001$, $n = 29$, Thymidine (Thy): $1.3x$, $r^2 = 0.91$, $p < 0.0001$, $n = 29$. BSB, Barents Sea shelf break; BSS, Barents Sea sector; CB, Central Arctic Basin; KSS, Kara Sea sector; LSB, Laptev Sea shelf break; LSS, Laptev Sea sector.

concentrations are expected to further decline due to shoaling of the mixed layer (Slagstad et al. 2015). Also changes in biological processes have the potential to affect the nitrate inventory of Arctic surface waters. An experimental study revealed that increasing light intensities as expected due to sea-ice reduction have a high potential to hamper nitrification above the upper halocline (Shiozaki et al. 2019). In line with this study, time-series observations in the Beaufort Sea showed decreasing shares of nitrifying *Thaumarchaeota* at reduced summer sea-ice concentrations (Comeau et al. 2011). As both nitrate supply by the Atlantic inflow and the replenishment by nitrification in the Arctic Ocean are expected to decrease, it can be suggested that negative effects of nutrient limitation on phytoplankton growth will counteract positive effects of higher light availability at reduced sea ice and, thereby, limit the accumulation of fresh DOM.

Spatial variability in concentration and composition of organic matter in the Eurasian Basin

Particulate organic matter showed similar surface concentrations in all regions of the Eurasian Basin despite spatial differences in Chl *a* and primary production. Average POC concentrations were about 30–45% lower than multiyear averages reported for the eastern Fram Strait but in the range of concentrations determined in the western Fram Strait (Engel et al. 2019; Nöthig et al. 2020). Different processes can serve as potential explanations for low concentrations and uniform distribution. Metazoan communities with high contributions of herbivores dominated the Atlantic regime in the Eurasian Basin and may have efficiently grazed particulate primary production (Flores et al. 2019). Also adaptations of phytoplankton to low light under ice and limiting nitrogen concentrations may have promoted low ratios of carbon to

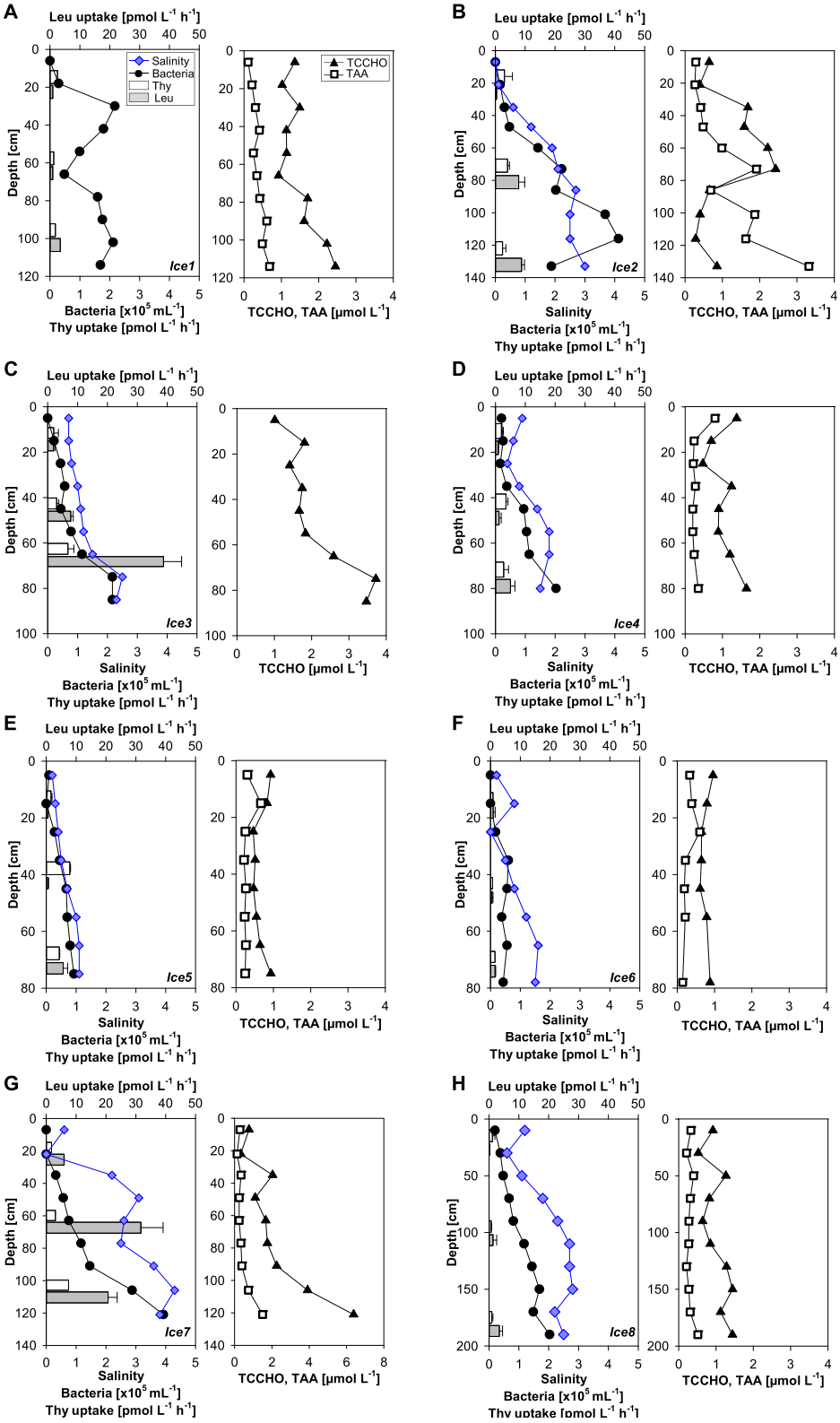

Fig 6. Ice-core profiles of salinity, bacterial cell numbers, bacterial activity, and organic matter concentrations. Leu, leucine uptake, TCCHO, total combined carbohydrates; Thy, thymidine; Leu, leucine. (A) Ice station 1, (B) Ice station 2, (C) Ice station 3, (D) Ice station 4, (E) Ice station 5, (F) Ice station 6, (G) Ice station 7, (H) Ice station 8.

Table 5. Depth-integrated bacterial biomass and activity in sea-ice cores.

Ice station	Ice type	Core length (cm)	Bacterial biomass (mg C m^{-2})	Bacterial production (μg C m^{-2} h^{-1})	Bacterial C demand (μg C m^{-2} h^{-1})
1	FYI	114	4.6	12.4	51.9
2	FYI	133	7.0	29.7	123.7
3	FYI	85	2.4	21.2	88.4
4	FYI	80	2.1	15.4	64.2
5	FYI	75	1.2	23.3	97.0
6	FYI	78	0.8	5.1	21.2
7	MYI	121	4.8	32.6	135.8
8	MYI	190	11.6	10.5	43.6

The bacterial carbon demand was estimated from bacterial biomass production assuming a bacterial growth efficiency of 24% according to Nguyen and Maranger (2011) (FYI, first-year ice; MYI, multiyear ice).

Chl *a* and enhanced exudation of photosynthesates (Harrison et al. 1990; Engel et al. 2011).

In contrast, DOM concentration and composition revealed clear regional differences. Higher loads of terrigenous DOC supplied by Siberian rivers and entrained into the Eurasian Basin resulted in significantly higher DOC concentrations in the upper water column (≤ 40 m) of the Laptev Sea sector and the central Arctic Basin than in the Barents Sea sector. It has been estimated that 60% of the DOC in the Laptev Sea and the adjacent Eurasian Basin originates from river discharge (Kattner et al. 1999). Studies investigating the reactivity of the terrigenous DOC in the Arctic Ocean came to divergent conclusions. Experiments with natural bacterial communities and in situ studies using isotopic tracers of water-mass age suggest long turnover times of several years (Hansell 2004; Meon and Amon 2004). This is supported by studies showing conservative mixing of riverine DOC in Arctic shelf seas (Kattner et al. 1999). However, other studies using similar approaches imply high initial lability of terrigenous DOC and substantial removal over the Siberian shelves (Alling et al. 2010; Letscher et al. 2011). In our study, DOC concentrations were inversely related to salinities of 30.0–34.3 at and beyond the Laptev Sea shelf break at 77.4°N–85.2°N and 110.1°E–131.8°E. The regression line deviates only slightly from a dilution line derived from previously published DOC concentrations in the Lena river (Lara et al. 1998). The extrapolated DOC concentration of 407 μmol L^{-1} for the freshwater endmember is in the range of values determined in the Lena river (300–1000 μmol L^{-1}, average 570 μmol L^{-1}; Lara et al. 1998). Hence, our results imply that the distribution of DOC in the Laptev Sea sector was largely driven by conservative mixing while only minor fractions of riverine DOC were remineralized before entrainment into the Eurasian Basin. It has been estimated that riverine freshwater contributes about 8% to the water budget at the Laptev Sea shelf break (Kattner et al. 1999). Given the average DOC concentration of 570 μmol L^{-1} reported for the Lena river by Lara et al. (1998), a fraction of 8% riverine freshwater would contain 46 μmol L^{-1} terrigenous DOC. This estimate of the terrigenous DOC supply at the Laptev Sea shelf break roughly equals the difference in DOC between the Barents Sea sector and the Laptev Sea sector and supports the conclusion that elevated DOC concentrations in the Laptev Sea sector primarily originated from riverine discharge.

Interestingly, surface waters of the Laptev Sea sector also showed significantly higher DAA concentrations than the other regions of the Eurasian Basin. Like DOC, also DAA concentrations were inversely related to salinity. Strong deviations of the regression line from the theoretical dilution line, however, suggest that DAA supplied by river discharge were efficiently remineralized during transport across the shelf. It is therefore likely that elevated DAA concentrations were derived from elevated primary production at low ice concentration in the Laptev Sea sector. Model projections reveal that the reduction of sea-ice coverage in the Laptev Sea sector by 50% between 1982 and 2012 resulted in 2.4 times higher primary production in late summer (Fernández-Méndez et al. 2015). The assumption that the DAA pool in the Laptev Sea sector was of marine origin is further supported by the amino acid composition. In the Lena river, DAA were shown to contain a substantially lower glycine proportion than surface seawater in our study (Lara et al. 1998). Therefore, a high contribution of riverine DAA to seawater would likely result in compositional differences between the sampling regions in the Eurasian Basin. However, PCA revealed a rather uniform DAA composition in the Eurasian Basin.

Table 6. Bacterial abundance and activity in melt ponds.

Bacteria ($\times 10^5$ mL^{-1})	Leu uptake (pmol L^{-1} h^{-1})	Thy uptake (pmol L^{-1} h^{-1})	Leu : Thy
1.31 (0.23–6.56)	6.21 (0.07–43.53)	0.48 (0.02–3.30)	12.4 (1.2–88.2)

The median is given as well as minimum and maximum values in parentheses (Leu, leucine; Thy, thymidine).

Environmental control of heterotrophic bacterioplankton in the Eurasian Basin

Comparing bacterial growth rates and biomass production in the Eurasian Basin with those in the eastern Fram Strait suggests that modification of Atlantic source waters in the Arctic Ocean strongly reduces the heterotrophic activity of bacterioplankton communities. Leucine uptake in the upper 5 m of the marginal ice zone (80°N–85°N) of the Eurasian Basin was about 3.5 times lower than in the West Spitsbergen Current at 79°N (Piontek et al. 2014). Based on the Q_{10} factor determined for bacterial leucine uptake in the upper water column of the Eurasian Basin, a temperature difference of 5.5°C as observed between the West Spitsbergen Current at 79°N and our study site would reduce leucine uptake by a factor of 1.6. Hence, the decrease in sea surface temperature alone cannot explain the decline in bacterial activity from the northern Fram Strait to the marginal ice zone in the Eurasian Basin. This finding supports the recent conclusion that seawater temperature is only one environmental factor among others that control bacterial growth in polar oceans (Kirchman et al. 2009; Ducklow et al. 2012; Piontek et al. 2015). Our results reveal a strong coupling of bacterial biomass production to primary production and phytoplankton standing stocks, suggesting that the availability of labile organic matter was an important constraint on heterotrophic bacterial activity. The average ratio of bacterial production to primary production was 0.11 in the Eurasian Basin at the time of our study and substantially higher than ratios in the western Arctic Ocean and other polar marine systems but in the range reported for the Equatorial Pacific and the subarctic North Pacific (Kirchman et al. 1993; Ducklow et al. 1995). Further evidence for a strong coupling between bacterial growth and phytoplankton dynamics is provided by the steep slope of the log-log regression between bacterial production and Chl *a*. The regression slope of 1.02 determined in our study is substantially higher than values previously reported for the Arctic Ocean (Cota et al. 1996; Nguyen et al. 2012; Ortega-Retuerta et al. 2014) and close to values derived from a global data set (Gasol and Duarte 2000). Overall, our results reveal that heterotrophic bacterial activity in the central Arctic Ocean was highly responsive to elevated primary production induced by light and nutrient availability and efficiently recycled primary production. Given this tight link, the flux of respiratory CO_2 from the ocean to the atmosphere may increase.

The efficient recycling of primary production in the Eurasian Basin suggests a successful adaptation of heterotrophic bacterial communities originating from Atlantic source waters to conditions in the central Arctic. Communities along the ice margin show similar ranges and median values for bacterial abundances, leucine, and thymidine uptake, suggesting similar potentials for heterotrophic bacterial carbon turnover despite pronounced differences in surface salinity and riverine DOC between Barents Sea sector and Laptev Sea sector. Comparing surface bacterioplankton communities reveals higher proportions of *Polaribacter* and *Formosa* in the Barents Sea sector than in the Laptev Sea sector at the time of our sampling (Rapp et al. 2018). Both genera belong to the class *Flavobacteriia* that is ubiquitous in the ocean and thrives on complex organic matter produced during phytoplankton blooms. Also previous studies reported on the high responsiveness of the genus *Polaribacter* to labile DOM derived from sea ice algae and phytoplankton in the Arctic Ocean (Yergeau et al. 2017; Dadaglio et al. 2019; Underwood et al. 2019). Communities in the Laptev Sea sector showed elevated proportions of the OM60/NOR5 clade (Balmonte et al. 2018; Rapp et al. 2018). Members of this clade have a photoheterotrophic metabolism that is regulated by the level of available carbon sources (Spring and Riedel 2013). These metabolic strategies of dominant community members in the Atlantic Water and in the Polar Mixed layer indicate that organic matter quality codetermined compositional shifts in bacterioplankton. Adaptations in community composition and metabolism may also explain regional differences in the ratio of leucine to thymidine uptake within the Eurasian Basin. Communities in the upper water column of the Laptev Sea sector and the central Arctic Basin showed significantly higher ratios than those in the Barents Sea sector, revealing that relatively more resources were allocated to biomass synthesis than to cell division in the Laptev Sea sector and the central Arctic Basin. An increase in leucine to thymidine uptake ratios was shown to co-occur with changes in the physiological state and/or unbalanced growth of cells in response to unfavorable conditions (Chin-Leo and Kirchman 1990). Hence, more unbalanced growth in the Laptev Sea sector and the central Arctic Basin may reflect changes in the community metabolism in response to the transition from Atlantic to Arctic conditions.

Organic matter distribution and heterotrophic bacterial activity in melting sea ice

Our results corroborate previous investigations that recognized the brine channel system as a substrate-rich habitat for heterotrophic bacteria (Thomas et al. 2001). Concentrations of TCCHO and TAA in ice cores were not correlated, suggesting that different processes determined the vertical and spatial distribution of the two compounds in sea ice. A potential explanation is the release of polysaccharide-enriched extracellular polymeric substances (EPS) that are important cryoprotectants produced by both autotrophic and heterotrophic sea-ice microbes (Meiners et al. 2008). Hence, EPS are partly released independent of primary production and can accumulate segregated from photosynthesates. The presence of glucuronic acid in sea-ice carbohydrates supports this assumption of significant EPS contribution. Uronic acids provide a structural element to EPS and contribute to some of the cell-protective properties (Steele et al. 2014). However, the uronic acid content of 1.0–4.7 mol% in our sea-ice samples was much lower than in previous studies that reported

37–48 mol% for Arctic and Antarctic sea ice (Underwood et al. 2013; Aslam et al. 2016). Instead, sea-ice carbohydrates were strongly dominated by glucose in our study. This difference may partly result from different analytical methods but could also be explained by changes in the carbohydrate composition during melting. Thicker ice was shown to contain relatively more particulate EPS, while thinner ice floes contained high amounts of glucose-rich dissolved carbohydrates (Aslam et al. 2016). Furthermore, the uronic acid content in EPS of sea-ice diatoms increased when seawater was cooled during experimental sea-ice formation (Aslam et al. 2018). These results suggest that the production of uronic acids by ice algae was potentially lower during the warm melting season, when our study took place.

Recent studies have demonstrated that the decline in sea ice leads to a substantial loss of bacterial diversity in the Arctic Ocean. Although originating from seawater, bacterial assemblages develop a unique composition after entrainment into newly formed ice (Hatam et al. 2016). In this study, mostly first-year ice floes strongly affected by melting were investigated. Abundances of sea-ice bacteria were in the range of published data for the Barents Sea and the Laptev Sea (Dahlbäck et al. 1982; Gradinger and Zhang 1997). The vertical distribution of sea-ice bacteria followed bulk salinity that gradually increased from top to bottom in most ice cores. Consequently, bottom ice showed the highest bacterial abundances but also top and middle sections comprised substantial proportions of sea-ice bacteria. The almost linear increase of bulk salinity from close to 0 at the ice surface up to 4.3 in the lower ice layers can be attributed to the replacement of brine by surface meltwater combined with convective overturning in lower ice parts that was triggered by increasing sea-ice permeability due to warming (Untersteiner 1968; Griewank and Notz 2013). Previous studies conducted during spring and early summer showed that bacterial biomass in first-year ice was almost exclusively confined to bottom ice in coincidence with maximum sea-ice algae biomass (Gosink et al. 1993). Hence, our results indicate that melting and related changes in bulk salinity induced shifts in the vertical distribution of bacterial biomass during late summer. As a consequence of the more homogenous vertical biomass distribution and similar salinity ranges in the ice cores, depth-integrated bacterial abundances were significantly correlated with the ice core lengths of 75–190 cm in our study. Extrapolating this relationship to ice floes, it can be suggested that ice melting during summer progressively reduced sea-ice bacterial biomass at a similar rate in the marginal ice zone of the Eurasian Basin during the last decades. Interestingly, the spatial variability of heterotrophic bacterial activity in sea ice did not resemble the distribution of bacterial biomass in our study. Instead, bacterial leucine uptake was directly related to concentrations of TCCHO that show a broad concentration range within and between ice cores. Carbohydrate-rich EPS have been identified as hot spots of bacterial respiration in sea ice (Meiners et al. 2008). The strong control of TCCHO on bacterial activity in our study supports the assumption that the EPS accumulation in sea ice promotes fast-growing bacteria like *Flavobacteriia* and *Gammaproteobacteria* that are specialized on the breakdown of polymeric organic compounds in the marine environment (Underwood et al. 2019). Although it must be assumed that the loss of bacterial biomass will ultimately constrain bacterial activity in melting sea ice, the decoupling of bacterial biomass from heterotrophic activity as observed in our study may mitigate the effect of biomass loss on heterotrophic bacterial carbon remineralization.

Surface ice melting leads to the formation of melt ponds on ice floes during summer. Increasing melt-pond coverage on Arctic sea ice draws the attention to this largely unknown microbial habitat (Brinkmeyer et al. 2004; Galgani et al. 2016; Rapp et al. 2018). While the composition of protist communities in melt ponds showed some overlap with sea ice, strong shifts in bacterial communities were observed (Hardge et al. 2017; Rapp et al. 2018). Bacterial communities were characterized by a stronger dominance of *Flavobacteriia* and higher shares of *Betaproteobacteria* compared to sea ice (Brinkmeyer et al. 2004; Rapp et al. 2018). Our results show that the melt pond-specific communities sustained higher rates of leucine and thymidine uptake than bacteria in the top and middle ice layers at most stations. Hence, adaptational shifts in the community composition allowed the re-establishment of growth in a new habitat (Rapp et al. 2018). Bacterial activity in melt ponds showed high variability that was likely related to the melt pond morphology. Shallow freshwater melt ponds without connection to the seawater below showed lower rates than those melt ponds that completely penetrated the ice and were more similar to the marine environment. The latter type of melt pond was characterized by higher salinity, primary production, and DOM concentrations (Fernández-Méndez et al. 2015; Galgani et al. 2016) and, thereby, likely represented a more favorable habitat for heterotrophic bacteria. Since about 20–50% of the ice surface area was covered with melt ponds in our study, it can be suggested that melt pond communities significantly contributed to bacterial carbon remineralization in the investigated Arctic first-year ice floes.

References

Alling, V., and others. 2010. Nonconservative behavior of dissolved organic carbon across the Laptev and East Siberian seas. Global Biogeochem. Cycles **24**: 1–15. doi:10.1029/2010GB003834

Arctic Climate Impact Assessment. 2004. Impacts of a warming Arctic: Arctic climate assessment. Cambridge Univ. Press.

Arnosti, C., A. D. Steen, K. Ziervogel, S. Ghobrial, and W. H. Jeffrey. 2011. Latitudinal gradients in degradation of

marine dissolved organic carbon. PLoS One **6**: 8–13. doi:10.1371/journal.pone.0028900

Arrigo, K. R., and G. L. van Dijken. 2015. Continued increases in Arctic Ocean primary production. Prog. Oceanogr. **136**: 60–70. doi:10.1016/j.pocean.2015.05.002

Aslam, S. N., C. Michel, A. Niemi, and G. J. C. Underwood. 2016. Patterns and drivers of carbohydrate budgets in ice algal assemblages from first year Arctic Sea ice. Limnol. Oceanogr. **61**: 919–937. doi:10.1002/lno.10260

Aslam, S. N., J. Strauss, D. N. Thomas, T. Mock, and G. J. C. Underwood. 2018. Identifying metabolic pathways for production of extracellular polymeric substances by the diatom *Fragilariopsis cylindrus* inhabiting sea ice. ISME J. **12**: 1237–1251. doi:10.1038/s41396-017-0039-z

Bakker, K. 2014. Nutrients measured on water bottle samples during POLARSTERN cruise ARK-XXVII/3 (IceArc) in 2012. PANGAEA. doi:10.1594/PANGAEA.834081

Balmonte, J. P., A. Teske, and C. Arnosti. 2018. Structure and function of high Arctic pelagic, particle-associated and benthic bacterial communities. Environ. Microbiol. **20**: 2941–2954. doi:10.1111/1462-2920.14304

Barlow, R. G., D. G. Cummings, and S. W. Gibb. 1997. Improved resolution of mono- and divinyl chlorophylls *a* and *b* and zeaxanthin and lutein in phytoplankton extracts using reverse phase C-8 HPLC. Mar. Ecol. Prog. Ser. **161**: 303–307. doi:10.3354/meps161303

Bidigare, R. R. 1991. Analysis of algal chlorophylls and carotenoids, p. 119–123. *In* D. C. Hurd and D. W. Spencer [eds.], Marine particles: Analysis and characterization. AGU. pp. 119–123.

Brinkmeyer, R., F. O. Glöckner, E. Helmke, and R. Amann. 2004. Predominance of β-proteobacteria in summer melt pools on Arctic pack ice. Limnol. Oceanogr. **49**: 1013–1021. doi:10.4319/lo.2004.49.4.1013

Carlson, C. A., and D. A. Hansell. 2014. DOM sources, sinks, reactivity, and budgets. *In* C. A. Carlson and D. A. Hansell [eds.], Biogeochemistry of marine dissolved organic matter. Academic Press. pp. 65–126. https://doi.org/10.1016/C2012-0-02714-7

Catalá, T. S., and others. 2016. Drivers of fluorescent dissolved organic matter in the global epipelagic ocean. Limnol. Oceanogr. **61**: 1101–1119. doi:10.1002/lno.10281

Chin-Leo, G., and D. L. Kirchman. 1990. Unbalanced growth in natural assemblages of marine bacterioplankton. Mar. Ecol. Prog. Ser. **63**: 1–8.

Comeau, A. M., W. K. W. Li, J. É. Tremblay, E. C. Carmack, and C. Lovejoy. 2011. Arctic Ocean microbial community structure before and after the 2007 record sea ice minimum. PLoS One **6**: e27492. doi:10.1371/journal.pone.0027492

Cota, G. F., L. R. Pomeroy, W. G. Harrison, E. P. Jones, F. Peters, W. M. Sheldon, and T. R. Weingartner. 1996. Nutrients, primary production and microbial heterotrophy in the southeastern Chukchi Sea: Arctic summer nutrient depletion and heterotrophy. Mar. Ecol. Prog. Ser. **135**: 247–258. doi:10.3354/meps135247

Dadaglio, L., J. Dinasquet, I. Obernosterer, and F. Joux. 2019. Differential responses of bacteria to diatom-derived dissolved organic matter in the Arctic Ocean. Aquat. Microb. Ecol. **82**: 59–72. doi:10.3354/ame01883. https://doi.org/10.1016/S0168-6496(99)00090-2

Dahlbäck, B., L. A. H. Gunnarsson, M. Hermansson,, and S. Kjelleberg. 1982. Microbial investigations of surface microlayers, water column, ice and sediment in the Arctic Ocean. Mar. Ecol. Prog. Ser. **9**: 101–109.

del Giorgio, P. A., and J. J. Cole. 1998. Bacterial growth efficiency in natural aquatic systems. Annu. Rev. Ecol. Syst. **29**: 503–541. doi:10.1146/annurev.ecolsys.29.1.503

Ducklow, H. W., H. L. Quinby, and C. A. Carlson. 1995. Bacterioplankton dynamics in the equatorial Pacific during the 1992 El Niño. Deep-Sea Res. Part II Top. Stud. Oceanogr. **42**: 621–638. https://doi.org/10.1016/0967-0645(95)00022-I

Ducklow, H. W., O. Schofield, M. Vernet, S. Stammerjohn, and M. Erickson. 2012. Multiscale control of bacterial production by phytoplankton dynamics and sea ice along the western Antarctic Peninsula: A regional and decadal investigation. J. Mar. Syst. **98–99**: 26–39. doi:10.1016/j.jmarsys.2012.03.003

Engel, A., and N. Händel. 2011. A novel protocol for determining the concentration and composition of sugars in particulate and in high molecular weight dissolved organic matter (HMW-DOM) in seawater. Mar. Chem. **127**: 180–191. doi:10.1016/j.marchem.2011.09.004

Engel, A., N. Händel, J. Wohlers, M. Lunau, H. P. Grossart, U. Sommer, and U. Riebesell. 2011. Effects of sea surface warming on the production and composition of dissolved organic matter during phytoplankton blooms: Results from a mesocosm study. J. Plankton Res. **33**: 357–372. doi:10.1093/plankt/fbq122

Engel, A., and others. 2019. Inter-annual variability of organic carbon concentration in the eastern Fram Strait during summer (2009–2017). Front. Mar. Sci. **6**: 1–17. doi:10.3389/fmars.2019.00187

Feller, G., and C. Gerday. 2003. Psychrophilic enzymes: Hot topics in cold adaptation. Nat. Rev. Microbiol. **1**: 200–208. doi:10.1038/nrmicro773

Fernández-Méndez, M., I. Peeken, and A. Boetius. 2014. Integrated net primary production during POLARSTERN cruise ARK-XXVII/3 (IceArc) in 2012. PANGAEA. doi:10.1594/PANGAEA.834218

Fernández-Méndez, M., C. Katlein, B. Rabe, M. Nicolaus, I. Peeken, K. Bakker, H. Flores, and A. Boetius. 2015. Photosynthetic production in the central Arctic Ocean during the record sea-ice minimum in 2012. Biogeosciences **12**: 3525–3549. doi:10.5194/bg-12-3525-2015

Flores, H., and others. 2019. Sea-ice properties and nutrient concentration as drivers of the taxonomic and trophic

structure of high-Arctic protist and metazoan communities. Polar Biol. **42**: 1377–1395. doi:10.1007/s00300-019-02526-z

Galgani, L., J. Piontek, and A. Engel. 2016. Biopolymers form a gelatinous microlayer at the air-sea interface when Arctic Sea ice melts. Sci. Rep. **6**: 1–10. doi:10.1038/srep29465

Gasol, J. M., and C. M. Duarte. 2000. Comparative analyses in aquatic microbial ecology: How far do they go? FEMS Microbiol. Ecol. **31**: 99–106. doi:10.1016/S0168-6496(99)00090-2

Gonçalves-Araujo, R., B. Rabe, I. Peeken, and A. Bracher. 2018. High colored dissolved organic matter (CDOM) absorption in surface waters of the central-eastern Arctic Ocean: Implications for biogeochemistry and ocean color algorithms. PLoS One **13**: 1–27. doi:10.1371/journal.pone.0190838

Gosink, J. J., R. L. Irgens, and J. T. Staley. 1993. Vertical distribution of bacteria in arctic sea ice. FEMS Microbiol. Lett. **102**: 85–90. doi:10.1016/0378-1097(93)90003-K

Gradinger, R., and Q. Zhang. 1997. Vertical distribution of bacteria in Arctic Sea ice from the Barents and Laptev Seas. Polar Biol. **17**: 448–454. doi:10.1007/s003000050139

Griewank, P. J., and D. Notz. 2013. Insights into brine dynamics and sea ice desalination from a 1-D model study of gravity drainage. J. Geophys. Res. Oceans **118**: 3370–3386. doi:10.1002/jgrc.20247

Hansell, D. A. 2004. Degradation of terrigenous dissolved organic carbon in the western Arctic Ocean. Science **304**: 858–861. doi:10.1126/science.1096175

Hardge, K., I. Peeken, S. Neuhaus, B. A. Lange, A. Stock, T. Stoeck, L. Weinisch, and K. Metfies. 2017. The importance of sea ice for exchange of habitat-specific protist communities in the Central Arctic Ocean. J. Mar. Syst. **165**: 124–138. https://doi.org/10.1016/j.jmarsys.2016.10.004

Harrison, P. J., P. A. Thompson, and G. S. Calderwood. 1990. Effects of nutrient and light limitation on the biochemical composition of phytoplankton. J. Appl. Phycol. **2**: 45–56. https://doi.org/10.1007/BF02179768

Hatam, I., B. Lange, J. Beckers, C. Haas, and B. Lanoil. 2016. Bacterial communities from Arctic seasonal sea ice are more compositionally variable than those from multi-year sea ice. ISME J. **10**: 2543–2552. doi:10.1038/ismej.2016.4

Holding, J. M., C. M. Duarte, A. Delgado-Huertas, K. Soetaert, J. E. Vonk, S. Agustí, P. Wassmann, and J. J. Middelburg. 2017. Autochthonous and allochthonous contributions of organic carbon to microbial food webs in Svalbard fjords. Limnol. Oceanogr. **62**: 1307–1323. doi:10.1002/lno.10526

Jeffrey, S. W., R. F. C. Mantoura, and T. Björnland. 1997. Data for the identification of 47 phytoplankton pigments, p. 449–559. *In* S. W. Jeffrey, R. F. C. Mantoura, and S. W. Wright [eds.], Pigments in oceanography: Guidelines to modern methods. Cambridge Univ. Press.

Jones, E. P., L. G. Anderson, and J. H. Swift. 1998. Distribution of Atlantic and Pacific waters in the upper Arctic Ocean: Implications for circulation. Geophys. Res. Lett. **25**: 765–768. https://doi.org/10.1029/98GL00464

Kattner, G., J. M. Lobbes, H. P. Fitznar, R. Engbrodt, E. M. Nöthig, and R. J. Lara. 1999. Tracing dissolved organic substances and nutrients from the Lena River through Laptev Sea (Arctic). Mar. Chem. **65**: 25–39. doi:10.1016/S0304-4203(99)00008-0

Kirchman, D., R. G. L. Keel, M. Simon, and N. A. Welschmeyer. 1993. Biomass and production of heterotrophic bacterioplankton in the oceanic subarctic Pacific. Deep-Sea Res. Part I Oceanogr. Res. Pap. **40**: 967–988. https://doi.org/10.1016/0967-0637(93)90084-G

Kirchman, D. L., B. Meon, H. W. Ducklow, C. A. Carlson, D. A. Hansell, and G. F. Steward. 2001. Glucose fluxes and concentrations of dissolved combined neutral sugars (polysaccharides) in the Ross Sea and Polar Front Zone, Antarctica. Deep-Sea Res. Part II Top. Stud. Oceanogr. **48**: 4179–4197. doi:10.1016/S0967-0645(01)00085-6

Kirchman, D. L., X. A. G. Morán, and H. Ducklow. 2009. Microbial growth in the polar oceans - role of temperature and potential impact of climate change. Nat. Rev. Microbiol. **7**: 451–459. doi:10.1038/nrmicro2115

Lara, J., V. Rachold, G. Kattner, H. W. Hubberten, G. Guggenberger, A. Skoog, and D. N. Thomas. 1998. Dissolved organic matter and nutrients in the Lena River, Siberian Arctic: Characteristics and distribution. Mar. Chem. **59**: 301–309. doi:10.1016/S0304-4203(97)00076-5

Lê, S., J. Josse, and F. Husson. 2008. FactoMineR: An R package for multivariate analysis. J. Stat. Softw. **25**: 1–18. doi:10.18637/jss.v025.i01

Letscher, R. T., D. A. Hansell, and D. Kadko. 2011. Rapid removal of terrigenous dissolved organic carbon over the Eurasian shelves of the Arctic Ocean. Mar. Chem. **123**: 78–87. doi:10.1016/j.marchem.2010.10.002

Lindroth, P., and K. Mopper. 1979. High performance liquid chromatographic determination of subpicomole amounts of amino acids by pre-column fluorescence derivatization with o-phthaldialdehyde. Anal. Chem. **51**: 1667–1674. doi:10.1021/ac50047a019

Meiners, K., C. Krembs, and R. Gradinger. 2008. Exopolymer particles: Microbial hotspots of enhanced bacterial activity in Arctic fast ice (Chukchi Sea). Aquat. Microb. Ecol. **52**: 195–207. doi:10.3354/ame01214

Meon, B., and R. M. W. Amon. 2004. Heterotrophic bacterial activity and fluxes of dissolved free amino acids and glucose in the Arctic Rivers Ob Yenisey and the Kara Sea. Aquat. Microb. Eol. **37**: 121–135. doi:10.3354/ame037121

Nguyen, D., and R. Maranger. 2011. Respiration and bacterial carbon dynamics in Arctic sea ice. Polar Biol. **34**: 1843–1855. https://doi.org/10.1007/s00300-011-1040-z

Nguyen, D., R. Maranger, J. É. Tremblay, and M. Gosselin. 2012. Respiration and bacterial carbon dynamics in the Amundsen Gulf, western Canadian Arctic. J. Geophys. Res. Oceans **117**: 1–12. doi:10.1029/2011JC007343

Nicolaus, M., C. Katlein, J. Maslanik, and S. Hendricks. 2012. Changes in Arctic Sea ice result in increasing light

transmittance and absorption. Geophys. Res. Lett. **39**: 1–6. doi:10.1029/2012GL053738

Niemi, A., G. Meisterhans, and C. Michel. 2014. Response of under-ice prokaryotes to experimental sea-ice DOM enrichment. Aquat. Microb. Ecol. **73**: 17–28. doi:10.3354/ame01706

Nöthig, E., and others. 2020. Summertime chlorophyll a and particulate organic carbon standing stocks in surface waters of the Fram Strait and the Arctic Ocean (1991–2015). Front. Mar. Sci. **7**: 1–15. doi:10.3389/fmars.2020.00350

Ortega-Retuerta, E., C. G. Fichot, K. R. Arrigo, G. L. Van Dijken, and F. Joux. 2014. Response of marine bacterioplankton to a massive under-ice phytoplankton bloom in the Chukchi Sea (Western Arctic Ocean). Deep-Sea Res. Part II Top. Stud. Oceanogr. **105**: 74–84. doi:10.1016/j.dsr2.2014.03.015

Oziel, L., and others. 2017. Oceans phytoplankton blooms in the Barents Sea. J. Geophys. Res. Oceans **122**: 5121–5139. doi:10.1002/2016JC012582

Parkinson, C. L., and C. Comiso. 2013. On the 2012 record low Arctic sea ice cover: Combined impact of preconditioning and an August storm. Geophys. Res. Lett. **40**: 1356–1361. doi:10.1002/grl.50349

Piontek, J., N. Händel, C. De Bodt, J. Harlay, L. Chou, and A. Engel. 2011. The utilization of polysaccharides by heterotrophic bacterioplankton in the Bay of Biscay (North Atlantic Ocean). J. Plankton Res. **33**: 1719–1735. doi:10.1093/plankt/fbr069

Piontek, J., M. Sperling, E. M. Nöthig, and A. Engel. 2014. Regulation of bacterioplankton activity in Fram Strait (Arctic Ocean) during early summer: The role of organic matter supply and temperature. J. Mar. Syst. **132**: 83–94. doi:10.1016/j.jmarsys.2014.01.003

Piontek, J., M. Sperling, E.-M. Nöthig, and A. Engel. 2015. Multiple environmental changes induce interactive effects on bacterial degradation activity in the Arctic Ocean. Limnol. Oceanogr. **60**: 1392–1410. doi:10.1002/lno.10112

Polyakov, I. V., and others. 2017. Greater role for Atlantic inflows on sea-ice loss in the Eurasian Basin of the Arctic Ocean. Science **356**: 285–291. doi:10.1126/science.aai8204

Polyakov, I. V., A. V. Pnyushkov, and E. C. Carmack. 2018. Stability of the arctic halocline: A new indicator of arctic climate change. Environ. Res. Lett. **13**: 125008. doi:10.1088/1748-9326/aaec1e

Qian, J., and K. Mopper. 1996. Automated high-performance, high-temperature combustion total organic carbon analyzer. Anal. Chem. **68**: 3090–3097. doi:10.1021/ac960370z

Quadfasel, D., A. Sy, D. Wells, and A. Tunik. 1991. Warming in the Arctic. Nature **350**: 385. https://doi.org/10.1038/350385a0

Rabe, B., A. Wisotzki, S. Rettig, R. Somavilla Cabrillo, and H. Sander. 2012. Physical oceanography during POLARSTERN cruise ARK-XXVII/3 (IceArc). Alfred Wegener Institute, Helmholtz Center for Polar and Marine Research. PANGAEA. doi:10.1594/PANGAEA.802904

Rapp, J. Z., M. Fernández-Méndez, C. Bienhold, and A. Boetius. 2018. Effects of ice-algal aggregate export on the connectivity of bacterial communities in the central Arctic Ocean. Front. Microbiol. **9**: 1035. doi:10.3389/fmicb.2018.01035

Riemann, B., R. Bell, and N. Jorgensen. 1990. Incorporation of thymidine, adenine and leucine into natural bacterial assemblages. Mar. Ecol. Prog. Ser. **65**: 87–94. doi:10.3354/meps065087

Rintala, J. M., J. Piiparinen, J. Blomster, M. Majaneva, S. Müller, J. Uusikivi, and R. Autio. 2014. Fast direct melting of brackish sea-ice samples results in biologically more accurate results than slow buffered melting. Polar Biol. **37**: 1811–1822. doi:10.1007/s00300-014-1563-1

Rudels, B. 2009. Arctic Ocean circulation. *In* J. Steele, S. Thorpe, and K. Turekian [eds.], Ocean currents: A derivative of the encyclopedia of ocean sciences. Academic Press. pp. 221–238.

Shiozaki, T., M. Ijichi, A. Fujiwara, A. Makabe, S. Nishino, C. Yoshikawa, and N. Harada. 2019. Factors regulating nitrification in the Arctic Ocean: Potential impact of sea ice reduction and ocean acidification. Global Biogeochem. Cycles **33**: 1085–1099. doi:10.1029/2018GB006068

Simon, M., and F. Azam. 1989. Protein content and protein synthesis rates of planktonic marine bacteria. Mar. Ecol. Prog. Ser. **51**: 201–213. doi:10.3354/meps051201

Slagstad, D., P. F. J. Wassmann, and I. Ellingsen. 2015. Physical constrains and productivity in the future Arctic Ocean. Front. Mar. Sci. **2**: 1–23. doi:10.3389/fmars.2015.00085

Smith, D. C., and F. Azam. 1992. A simple, economical method for measuring bacterial protein synthesis rates in seawater using tritiated-leucine. Mar. Microb. Food Webs **6**: 107–114.

Smith, R. E. H., and P. Clement. 1990. Heterotrophic activity and bacterial productivity in assemblages of microbes from sea ice in the high Arctic. Polar Biol. **10**: 351–357. doi:10.1007/BF00237822

Sperling, M., J. Piontek, A. Engel, K. H. Wiltshire, J. Niggemann, G. Gerdts, A. Wichels, and J. A. Fonvielle. 2017. Combined carbohydrates support rich communities of particle-associated marine bacterioplankton. Front. Microbiol. **8**: 1–14. doi:10.3389/fmicb.2017.00065

Spring, S., and T. Riedel. 2013. Mixotrophic growth of bacteriochlorophyll a-containing members of the OM60 / NOR5 clade of marine gammaproteobacteria is carbon-starvation independent and correlates with the type of carbon source and oxygen availability. BMC Microbiol. **13**: 117. https://doi.org/10.1186/1471-2180-13-117

Steele, D. J., D. J. Franklin, and G. J. C. Underwood. 2014. Protection of cells from salinity stress by extracellular polymeric substances in diatom biofilms. Biofouling **30**: 987–998. doi:10.1080/08927014.2014.960859

Steemann Nielsen, E. 1952. The use of radio-active carbon (C14) for measuring organic production in the sea. ICES

J. Mar. Sci. **18**: 117–140. https://doi.org/10.1093/icesjms/18.2.117

Sugimura, Y., and Y. Suzuki. 1988. A high-temperature catalytic oxidation method for the determination of non-volatile dissolved organic carbon in seawater by direct injection of a liquid sample. Mar. Chem. **24**: 105–131. https://doi.org/10.1016/0304-4203(88)90043-6

Thomas, D. N., G. Kattner, R. Engbrodt, V. Giannelli, H. Kennedy, C. Haas, and G. S. Dieckmann. 2001. Dissolved organic matter in Antarctic Sea ice. Ann. Glaciol. **33**: 297–303. doi:10.3189/172756401781818338

Underwood, G. J. C., and others. 2013. Broad-scale predictability of carbohydrates and exopolymers in Antarctic and Arctic Sea ice. Proc. Natl. Acad. Sci. USA **110**: 15734–15739. doi:10.1073/pnas.1302870110

Underwood, G. J. C., C. Michel, G. Meisterhans, A. Niemi, C. Belzile, M. Witt, A. J. Dumbrell, and B. P. Koch. 2019. Organic matter from Arctic Sea-ice loss alters bacterial community structure and function. Nat. Clim. Chang. **9**: 170–176. doi:10.1038/s41558-018-0391-7

Untersteiner, N. 1968. Natural desalination and equilibrium salinity profile of perennial sea ice. J. Geophys. Res. **73**: 1251–1257. https://doi.org/10.1029/JB073i004p01251

Yager, P. L., and J. W. Deming. 1999. Pelagic microbial activity in an arctic polynya: Testing for temperature and substrate interactions using a kinetic approach. Limnol. Oceanogr. **44**: 1882–1893. doi:10.4319/lo.1999.44.8.1882

Yergeau, E., C. Michel, J. Tremblay, A. Niemi, T. L. King, J. Wyglinski, K. Lee, and C. W. Greer. 2017. Metagenomic survey of the taxonomic and functional microbial communities of seawater and sea ice from the Canadian Arctic. Sci. Rep. **7**: 1–10. doi:10.1038/srep42242

Acknowledgments

We would like to thank the captain and the crew of *RV* Polarstern and the shipboard science party of the expedition IceArc (PS80, ARK XXVII/3) for their great support during the cruise. Our special thanks go to Catherine Lalande, Christiane Uhlig, Anique Stecher, and Mar Fernández-Méndez for their help in sampling and excellent support during work on ice floes. Christiane Lorenzen, Jon Roa, Ruth Flerus, and Tania Klüver are greatly acknowledged for their help with sample analyses. Our thanks go to Karel Bakker for nutrient analysis. We also thank Sebastian Albrecht for providing the sea-ice map used in Fig. 1. This work was financed by the institutional funds of the GEOMAR Helmholtz Centre for Ocean Research Kiel, and by the programme Polar Regions and Coasts in a Changing Earth System (PACES) of the Helmholtz Association. JP was supported by the DFG grant PI 784/3-1. This study is also a contribution to the BMBF funded project MicroARC (03F0802A). Open access funding enabled and organized by Projekt DEAL.

Conflict of Interest

None declared.

Submitted 25 February 2020
Revised 09 July 2020
Accepted 22 September 2020

Associate editor: Ronnie Glud